

# Axial Rotation and Lateral Torsional Buckling of Extruded Aluminium Mullions in Curtain Wall Facades

Adam D. Lee<sup>a,b,\*</sup>, Jed A. Alimanza<sup>b</sup>, Paul Shepherd<sup>a</sup>, Mark C. Evernden<sup>a</sup>

<sup>a</sup>*Department of Architecture and Civil Engineering, University of Bath, Claverton Down, Bath, BA2 7AY, U.K.*

<sup>b</sup>*PTCC Facade Design, Telecom Plaza, 316 Senator Gil Puyat Ave., Makati City, Metro Manila, 1200, Philippines.*

---

## Abstract

Large modern buildings frequently are enclosed by lightweight, panelised, aluminium-framed facades, known as unitised curtain walls. This study shows that, in such wall systems, the established procedures for analysing the stability of structural extrusions ignore two of the three greatest causes of lateral movement in the main member, or mullion. One of these overlooked influences is the force caused by the pressurisation of the mullion's interior cavity, and the other is the moment transferred to the mullion, through structural adhesive, from the wall's face material, which is usually glass.

A new, closed-form, algebraic expression is proposed to describe the lateral movement of a unitised mullion's interior flanges, and predictions obtained in this way are compared with results from a finite element model. It is suggested that the novel analytical approach might obviate the need for conventional lateral torsional buckling calculations, which are not only time-consuming to produce, but which are also of questionable accuracy. This simplification of the structural design process will make it easier for facade engineers to design extrusions in which metal is used efficiently, and because the production of aluminium is energy-intensive, material savings achieved in this way will bring both

---

\*Corresponding Author

*Email addresses:* [adamlee@torstencalvi.com](mailto:adamlee@torstencalvi.com) (Adam D. Lee), [jedalimanza@torstencalvi.com](mailto:jedalimanza@torstencalvi.com) (Jed A. Alimanza), [p.shepherd@bath.ac.uk](mailto:p.shepherd@bath.ac.uk) (Paul Shepherd), [m.evernden@bath.ac.uk](mailto:m.evernden@bath.ac.uk) (Mark C. Evernden)

<http://dx.doi.org/10.1016/j.istruc.2019.05.010>

© 2019. This manuscript version is made available under the CC-BY-NC-ND 4.0 license <http://creativecommons.org/licenses/by-nc-nd/4.0/>

*Preprint submitted to Elsevier "Structures"*

*May 20, 2019*

commercial and environmental benefits.

*Keywords:* curtain wall, mullion, facade design, aluminium extrusions, structural stability, lateral torsional buckling

---

## Notation

$a$	Length of longer side of structural plate or glass pane. [Length]
$\beta$	$\sqrt{\frac{J_{zz:m}G_a}{C_w E_a}}$ . [Length <sup>-1</sup> ]
$b$	Length of shorter side of structural plate or glass pane, or horizontal distance between adjacent mullions. [Length]
$b_m$	Combined width, or breadth, of the profiles in a split mullion. [Length]
$B$	Width of contact surface, or bite, between structural silicone sealant and substrate. [Length]
$C_b$	Equivalent uniform moment factor for a flexural member [1, Fig. 5.8]. [Dimensionless]
$C_{bb}$	Moment modification factor for full bracing condition, which is the value of $C_b$ achieved when bracing is fully effective 2. [Dimensionless]
$C_w$	A mullion profile's warping constant. [Length <sup>6</sup> ]
$\delta_x$	A mullion's deflection in the direction perpendicular to the plane of the wall, measured with respect to the transoms at the ends of the unbraced span. [Length]
$\delta'_x, \delta'_y$	A mullion's horizontal deflections in the directions parallel to its strong and weak principal axes respectively. [Length]
$\delta_{x:a}$	Horizontal deflection of a mullion profile's interior flange in the direction parallel to the plane of the wall, caused by asymmetric bending. [Length]
$\delta_{x:b}$	The horizontal deflection, in the plane of the wall, of a mullion profile bending about its $y$ -axis because of loads caused by pressure equalisation. [Length]
$\delta_{x:r}$	The horizontal deflection, in the plane of the wall, of a mullion's interior flange, due to rotation about the longitudinal- or $z$ -axis caused by wind loads upon the webs and flanges. [Length]

$\delta_{x:s}$	The horizontal deflection of a mullion's interior flange, resulting from the combined bending and rotation caused by wind load upon the webs and flanges. [Length]
$d_m$	A mullion's depth or distance between the extreme fibers of the interior and exterior flanges (approximately equal to the distance from face of exterior flange to the air seal, and approximately equal to the distance between the centroids of the two inner and outer flanges.) [Length]
$d_s$	The horizontal distance, in the direction perpendicular to the wall, from a mullion extrusion's shear centre to the extreme fiber on the interior side.
$D$	Flexural rigidity of a plate or glass pane. [Force $\times$ Length]
$e_{sx}$	The horizontal distance, in the direction parallel to the wall, from a mullion extrusion's shear centre to the point at which load is applied to its exterior flange.
$e_{sy}$	The horizontal distance, in the direction perpendicular to the wall, from a mullion extrusion's shear centre to the midpoint between its exterior extreme fiber and interior air seal.
$E$	Young's modulus. [Force/Length <sup>2</sup> ]
$E_a$	Young's modulus of aluminium. [Force/Length <sup>2</sup> ]
$E_s$	Young's modulus of structural silicone sealant. [Force/Length <sup>2</sup> ]
$g$	Thickness, or "glueline", in the direction normal to the contact surface, in a structural silicone sealant joint. [Length]
$G_a$	Shear modulus of aluminium. [Force/Length <sup>2</sup> ]
$I_{xx}, I_{yy}$	A flexural member's second moment of area in bending about the centroidal axes that are parallel and perpendicular to the wall, respectively. [Length <sup>4</sup> ]
$I_{xy}$	A flexural member's product moment of area with respect to the centroidal axes that are parallel and perpendicular to the wall. [Length <sup>4</sup> ]
$I_{xx:m}, I_{yy:m}$	A mullion profile's second moment of area about the centroidal axes that are parallel and perpendicular to the wall, respectively. [Length <sup>4</sup> ]
$I'_{xx:m}, I'_{yy:m}$	A mullion profile's second moment of area about its strong and

	weak centroidal principal axes, respectively. [Length <sup>4</sup> ]
$I_{xx:t}$	A transom profile's second moment of area about the centroidal axis that is parallel to the wall. [Length <sup>4</sup> ]
$I_{yy:e}$	A mullion profile's effective second moment of area about the centroidal axis that is perpendicular to the wall. [1, p. 551-552]. [Length <sup>4</sup> ]
$J_{zz:m}$	Torsion constant of a mullion profile's cross-sectional shape [e.g. 3, Part II, Chapter B.1]. [Length <sup>4</sup> ]
$k$	Temporary constant used during asymmetric bending calculation. [Force/Length <sup>2</sup> ]
$k_{mf}$	Multiplicative factor used to set the polarity of deflection with respect to mullion centreline. Viewed from exterior of building, $k_{mf} = 1$ and $k_{mf} = -1$ for the right and left hand profiles respectively. [Dimensionless]
$l_b$	A mullion's unbraced span, meaning the clear distance between transom members. [Length]
$M_{x:m}$	Maximum permissible moment in a mullion, acting about the centroidal axis that is parallel to the wall, when the member is braced to prevent lateral torsional buckling. [Force $\times$ Length]
$M_{z:b}$	The moment, acting about a mullion's longitudinal- or $z$ -axis, carried by a torsional brace that is capable of preventing lateral torsional buckling. [Force $\times$ Length].
$M_{z:p}$	The moment, acting about a mullion's longitudinal- or $z$ -axis, caused by pressure equalisation. [Force $\times$ Length].
$M_{z:s}$	Moment transferred to a mullion profile through structural silicone sealant, and acting about the member's longitudinal- or $z$ -axis. [Force $\times$ Length]
$\nu$	Poisson's ratio. [Dimensionless]
$P$	Pressure. [Force/Length <sup>2</sup> ]
$q$	Load, per unit length of member, acting in the direction perpendicular to the wall. [Force/Length]
$\theta_{z:b}$	Maximum angular deflection of a mullion profile about a longitudinal- or $z$ -axis, due to lateral torsional buckling effects. [Radians]
$\theta_{z:g}$	Maximum angular deflection of mullion, due to in-plane movement of glass edge. [Radians]

$\theta_{z:p}$	Maximum angular deflection of a mullion profile about a longitudinal- or z-axis, due to moment about that axis caused by wind load upon webs and flanges. [Radians]
$\theta_{z:t}$	Maximum angular deflection of a mullion profile about a longitudinal- or z-axis, due to rotation of an attached transom. [Radians]
$t$	Thickness of plate or glass pane. [Length]
$u$	In-plane displacement of edge of plate or glass pane. [Length]
$w$	Out-of-plane deflection of plate or glass pane. [Length]
$w_{max}$	Maximum out-of-plane deflection of plate or glass pane. [Length]

## 1. Introduction

In 1996, a typical fabricator of architectural glass could supply heat treated panes with a long dimension of 4 m, and the largest size available in the industry was 5 m [4, p. 275]. By 2007 the maximum had risen to somewhere in excess of 6 m [5, p. 55], and today it is not uncommon to find panes exceeding 10 m. At least two firms now are capable of heat treating pieces of glass up to 16 m in length [6, 7].

These advances within the glass processing industry have occurred in response to architectural demand. Larger panes are desirable because, with fewer glass joints in a facade, a building's occupants can enjoy a greater unobstructed view of their exterior surroundings. So, in curtain walls – the sort of lightweight, metal-framed exterior enclosures that are, today, routinely used to sheath high-rise commercial towers – the result is an increase in the unsupported distances spanned by the metal framing members that surround the glass panes. Structurally, these members, which are almost invariably aluminium extrusions, have become more slender.

A second trend, a change in the way that curtain wall systems are manufactured and installed, has further increased the slenderness of the structural profiles. Since their introduction in the 1960s [8], growth in the use of ‘unitised’ curtain walls, made up of discrete, prefabricated panels, has been much more

rapid than growth in the use of the previously dominant ‘stick’ curtain walls, which are assembled at the construction site from box-like extrusions. Examples of stick and unitised wall systems are shown in Figure 1. By 2012, in the world-wide market, the area of facade constructed from unitised systems was twice that constructed from stick systems [9, p.82]. Because the vertical members in the unitised wall are in two interconnecting parts, each individual extrusion is less wide than the mullion in the stick curtain wall.

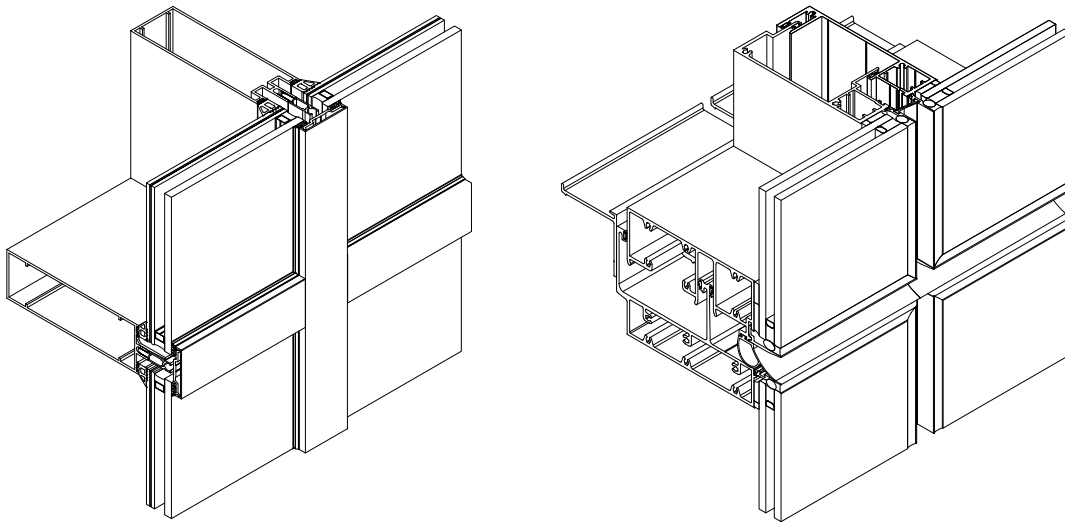


Figure 1: The box mullion and box transom in stick curtain wall (left) and the split mullion and stack joint of a unitised curtain wall (right).

Of the different stresses induced in a mullion, by far the most significant are those caused by the action of wind upon the exterior surface of the wall. The mullion is placed in flexure, and so, even though its extrusion axis is vertical, in structural terminology, it is a beam. At points of connection with the curtain wall’s horizontal members, the ‘transoms’, the mullion can move in the direction perpendicular to the wall, but rotation about its longitudinal axis is restrained by the transom, as described in Section 2.7. Away from the transoms, however, internal or applied forces can cause rotation. Each of these conditions is illustrated in Figure 2.

In the structural analysis of a curtain wall mullion, it is the convention to

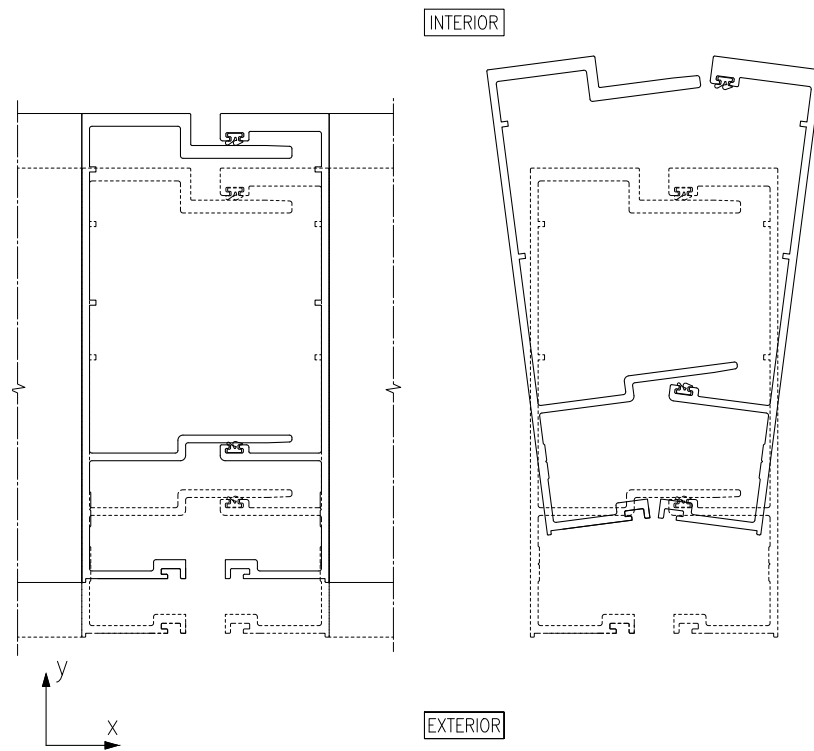


Figure 2: Plan view of unutilised curtain wall mullion at connection with mullion (left) and at mid span (right), without load (dashed line) and with rotation in response to applied wind load (solid line).

assume that load is applied only in a plane parallel to the member's web, and that the 'infill' material – the glass or metal sheet that forms the exterior surface of the wall – does not provide bracing [e.g. 10]. A facade designer must check, by calculation, that neither the flanges nor the webs of proposed mullion cross sections are too thin to resist local buckling, a mode of failure in which one or more elements of the extrusion take on an undulating shape, these undulations having a wavelength much smaller than the member's span. The structural design codes [e.g. 11, Section B.5.4] provide simple calculation methods with which to assess a profile's resistance to local buckling. However, if the member is slender then further checks must be made to ensure that, when the design moment is applied, rotation of the cross section in the central part of the span will not cause instability. This second mode of failure, lateral torsional buckling (LTB), is described diagrammatically in Figure 2. Because the mullions of modern unitised curtain wall systems are becoming more slender, LTB is often the governing consideration in their structural design.

The analysis of a proposed mullion's resistance to LTB is complex and can be time consuming. If the rules of a popular design code, the Aluminium Design Manual (ADM) [11], are observed, then aside from the various properties of the cross section that must be found, a moment distribution coefficient must be determined for each unsupported span. A single curtain wall panel may have multiple inter-transom spans and, for each span, the LTB resistance of the male and the female profile have to be assessed independently. Further, because the direction of load affects a member's buckling strength, it is necessary to consider separately the cases in which wind pressure is positive, acting toward the wall, and also negative, acting away from the wall. Even if some or all of the analysis can be automated using software, the computations must still be presented in a human-readable format so that they can be checked by peers, and so extensive calculation reports may be needed to demonstrate that all of the mullions in a building's facade are adequately stable. For example, during a recent curtain wall design project in which the lead author was involved, the stability analysis of mullion extrusions in a laboratory test specimen, which contained only 16



panels, ran to more than 400 pages of typeset algebra and tables. That particular set of computations followed the procedures set out in the ADM, but the LTB analysis methods provided in other structural design codes are similarly cumbersome. Skejić et al. remarked that the method defined in the European design standard, EN 1999-1-1, for the analysis of LTB in unitised curtain wall mullions, is “a long and complicated procedure for non-symmetrical sections which makes it pretty impractical” [12].

An alternative means of investigating the stability limits of a given set of curtain wall extrusions is to create a finite element model of the structural system. A numerical study of this sort is described in Section 4. For research purposes, or to investigate the behaviour of a few special conditions in a building facade, finite element modelling is a powerful tool. However, to create sufficiently detailed models, and to process those models using iterative, non-linear algorithms, can be a lengthy and computationally demanding process. This, therefore, is not a practical means of assessing the large numbers of different mullion configurations that may be present in a real facade. Whether LTB is modelled numerically or analytically, it is a costly part of the curtain wall design process.

Despite all of the effort that is expended to check that the stresses in framing members will not go beyond the codified LTB limits, it is not clear that the mullion in a real curtain wall would necessarily become unstable if those limits were exceeded. CWCT, a facade industry standards body, while acknowledging that mullions are becoming more slender, and while officially recommending that all mullions should comply with the analytical rules for LTB, notes that “lateral torsional buckling is not known to have caused failure of curtain walling either in service or under test conditions” [10]. Clift [13] and Goco [14] have shown that, if the support given to the mullion by the glass or infill material were acknowledged in the LTB analysis, then a slender mullion’s theoretical moment capacity would increase significantly. Skejić and coauthors [12] used the finite element method to model buckling in a particular unitised mullion, and concluded that the member’s actual moment capacity was several times greater, and possibly as

much as an order of magnitude greater, than the moment capacity predicted by code. These observations suggest that the current methods of determining LTB resistance are, at least in some cases, unduly conservative.

A slender mullion's cross-sectional shape and its moment resistance are related by mathematical expressions that are complex [e.g. 11, Part I, Section F4]. The level of complexity is such that it is difficult, even for experienced curtain wall designers, to find the number, configuration and sizes of flanges and webs needed to satisfy the structural performance criteria while at the same time minimising the quantity of aluminium in the wall. The consequence is that, even when a custom curtain wall system is developed for a specific project, it is common that aluminium is used inefficiently [15]. If building facades contain more metal than is structurally necessary, current LTB analysis techniques may be partly to blame, not just because the codes' demands are conservative, but, in addition, because the complexity of their formulation is a barrier to efficient design. In construction it is desirable to minimise the usage of every type of material, and there is an obvious commercial motive to do so. When the material in question is aluminium, which is produced by methods that are unusually energy intensive [16, p. 32], for environmental reasons the metal should be used sparingly. In a previous study [17], an attempt was made to estimate the scale of the cost savings, and also the scale of the reduction in greenhouse gas emissions, that might be achieved if effective structural optimisation methods were to be applied by the world's curtain wall designers. The potential benefits are substantial.

The mullion is the curtain wall panel's principal structural member, but it also serves other, non-structural purposes. For example, if the wall is to function as a weather barrier, the male and female extrusions must engage with one another to maintain an air-tight seal. If wind load causes the profiles to rotate in the manner indicated in Figure 2 then, as the two interior flanges move further apart, the air seal will fail. Even if both of the profiles in a split mullion satisfy the codified analytical criteria for LTB resistance, it does not necessarily follow that, when load is applied, their rotation will be too small

to cause disengagement. The authors are aware of anecdotal but technically plausible accounts of pre-construction structural tests, simulating the action of wind load on prototype curtain wall panels, that were said to fail in this way, even though analysis had shown that the design load would not cause LTB. Witnesses said that the split mullions oscillated between the open and closed position, like the reeds in musical instruments, creating a loud purring noise.

One means of limiting the extent to which the two sides of the split mullion can separate, and hence avoid a breach of the air seal, is to introduce mechanical latches known as ‘anti-buckling clips’. Two such designs are shown in Figure 3. Although they are included in many modern curtain wall systems, their effectiveness in their nominal ‘anti-buckling’ role is unclear. While the inclusion of anti-buckling clips does prevent separation of the interior air seal, there may be practical reasons for designing without them. One of the disadvantages is that, if the clip extrusions are separate from the mullions, they add to design complexity, material cost and fabrication time. Another issue is that, during normal building movements, metal-to-metal contact at clips may create unwelcome noise. A third potential problem is that, if a panel is installed incorrectly, it can be difficult or impossible to separate it from its neighbour without permanently damaging the mullion.

For the purpose of LTB analysis, it is the convention to assume that the mullion sections are restrained only at transom locations, and that all structural responses are attributable to a line load acting upon the outer flange, in the direction perpendicular to the wall, as indicated in the diagram at the right hand side of Figure 4. This present study considers forces that are neglected in the standard model, but which, in practice, influence the lateral movement of member’s flanges. To model each of these effects, short, closed-form algebraic expressions are proposed in Section 2. The design of a real building’s curtain wall is detailed in Section 3, and a finite element study of this wall specimen is described in Section 4. The results of the finite element study have been used to validate the algebraic predictions and, in Section 5, the mathematical models of the different physical phenomena are combined in a closed-form expression.

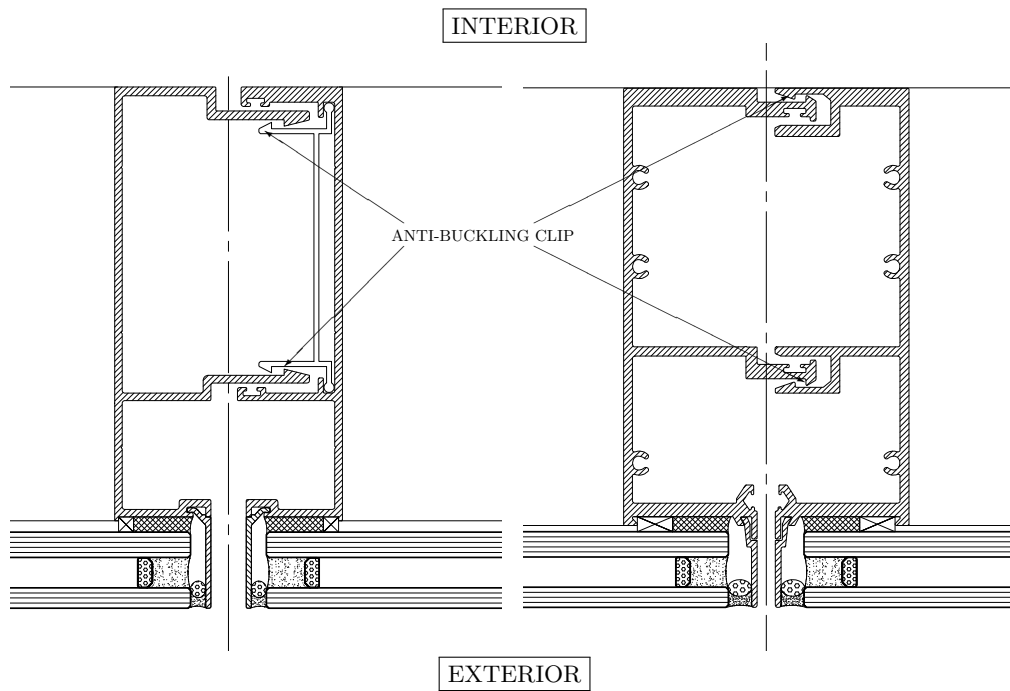


Figure 3: Split mullion with local 'anti-buckling clip' extrusion (left), and split mullion with continuous integral clips (right [18]).

It is hoped that these new insights into the loads that act upon real curtain wall mullions, and the new models that describe the mullions' responses to the loads, will help curtain wall designers to shape their structural extrusions in such a way that aluminium is used efficiently.

## **2. The Causes of Mullion Flange Movement in Plane of Wall**

The different physical effects that cause the interior flanges of mullion extrusions to move laterally, in the plane of the wall, are examined below. The mathematical expressions presented here are intended to describe the behaviour of mullions in a wide range of unitised curtain wall designs and, by inserting the applicable material properties, can be applied to extrusions of any particular aluminium alloy and temper.

### *2.1. Lateral Torsional Buckling*

It is easy to visualise the wind pressure acting upon the exterior surface of a curtain wall, causing a line load to act upon the mullion's outer flange and, hence, bending about the strong- or  $x$ -axis. Even if, in accordance with the established facade design convention, other applied loads are ignored, the bending moments induced in the split mullion by wind pressure can cause the profiles to rotate about a longitudinal axis. The processes that cause this rotation are complex. In codified approaches to the analysis of a beam's stability, the compression flange is considered to behave as an Euler column, which is free to deflect and buckle laterally. In reality, other phenomena, some of which are outlined below, also cause the cross section to rotate.

It is a corollary of the classical, small-deflection beam analysis theory of Euler [19, 20] and Bernoulli [21, pp.30-36] that the stresses in the fibers of a flexural member vary in proportion with their distance from the elastic neutral axis. In reality, however, shear lag causes the stress and strain in a flange to diminish with distance from the web and, as a result, a flange that is not symmetrical about the web will deflect laterally. In the diagram on the left-hand of Figure 4, it can be seen that this effect can cause the whole cross

section to rotate. Changes in the profile's cross-sectional shape, exaggerated in the central sketch in Figure 4, further complicate the geometry and hence the analysis. Also, as the cross section rotates in the manner sketched on the right hand side of Figure 4, so the eccentricity of the applied load increases.

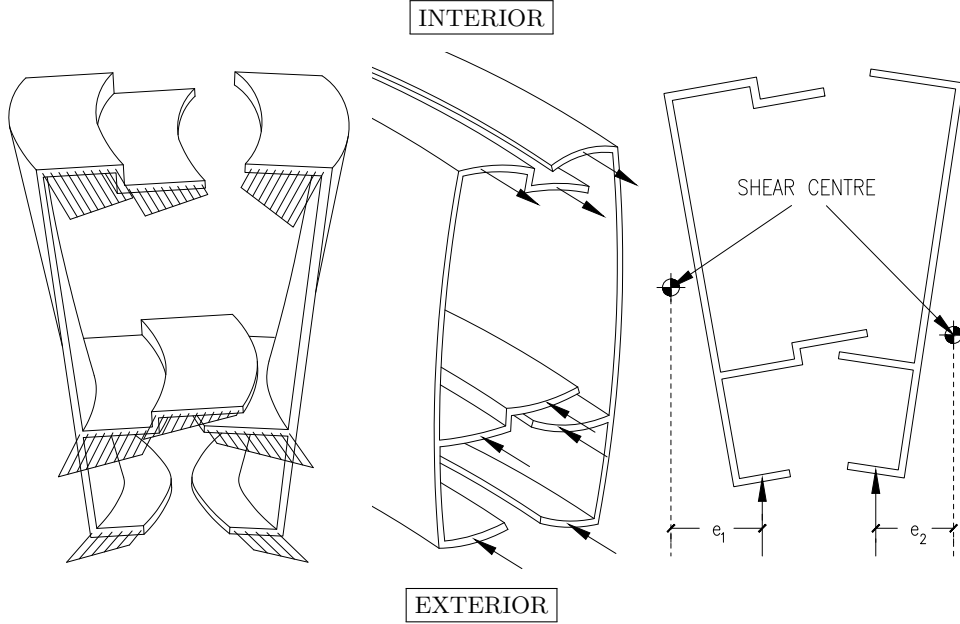


Figure 4: Shear lag causes mullion in flexure to rotate (left). Bending stresses in flanges cause deflection in the plane of the cross section (centre). Eccentricity of applied load changes as member rotates (right).

The Structural Stability Research Council [1, Equation 12.10; 2] advises that, if it is to be effective in preventing LTB, the minimum unfactored torsional stiffness of a continuous brace (expressed as a moment per unit length of member, per radian of axial rotation at the centre of the span),  $M_{z:b}/\theta_{z:b}$ , with some changes to the original variable names, is:

$$\frac{M_{z:b}}{\theta_{z:b}} = \frac{2.4M_{x:m}^2}{E_a I_{yy:e} C_{bb}^2}, \quad (1)$$

where  $M_{x:m}$  is the maximum design moment about the  $x$ -axis, and  $E_a$  is the Young's modulus of the member, which, in the current context, is made of aluminium. The meanings and the usage of the other terms,  $I_{yy:e}$  and  $C_{bb}$ , are

explained in the paragraphs that follow.

$C_{bb}$  is the moment modification factor for the full bracing condition. In other words,  $C_{bb}$  is the value of the equivalent uniform moment factor,  $C_b$  [1, Fig. 5.8], assuming that the bracing is fully effective. In the worked examples that follow, the value of  $C_{bb}$  is taken to be 2.0 when the interior flange is in tension and also when it is in compression, which implies that the mullion's outer flange is laterally restrained by its connection to the glass.

The value of  $I_{yy:e}$ , which is the effective second moment of area about an axis that is perpendicular to the wall and passing through the centroid, will be equal to the second moment of area about the weak- or  $y$ -axis,  $I_{yy:m}$ , only if the profile's centroid lies exactly mid way between the inner and outer flanges. A method for calculating  $I_{yy:e}$  is provided by Ziemeian [1, p. 551-552], however, for the purpose of this study an approximation is sufficient, so it will be assumed that  $I_{yy:e} \approx I_{yy:m}$ . Equation 1 applies to the more severe case in which loads applied at a flange act toward, rather than away from, the profile's centroid. The expression was originally derived for beam sections having at least one axis of symmetry, and its applicability to a doubly-asymmetric mullion profiles is discussed in Section 6.2.

The minimum unfactored ultimate strength of the torsional brace [2, p. 15] (a moment per unit length of member) is:

$$M_{z:b} = \frac{0.04M_{x:m}^2}{E_a I_{yy:e} C_{bb}^2} . \quad (2)$$

The axial moment that is required to prevent LTB in the mullion profiles of a given curtain wall can be estimated using Equation 2. The magnitude of the moment is of interest because, in this paper, it will be compared with the other moments acting about a mullion profile's longitudinal axis. Similarly, the torsional stiffness of a mullion extrusion's connection to its adjacent structural components will be compared with the minimum stiffness of a torsional brace, which can be found with Equation 1.

## 2.2. Rotation Due to Wind Loads on Flanges and Webs

One of the methods used to prevent the passage of water through the inter-panel joints in a unitised curtain wall is to ‘pressure equalise’ [22, 23] some or all of the cavities inside the framing members. These cavities are open, or partially open, to the exterior side of the wall, and cavity pressure varies with the exterior wind pressure. In practice, when the exterior wind load fluctuates rapidly, the response measured within the cavity may be damped and attenuated, and so it is conservative to assume that the cavity pressure is equal to the wind load. A consequence of pressure equalization is that forces act upon a mullion profile’s web and interior flange and the member experiences a lateral force in the plane of the wall, as well as a moment about its longitudinal axis.

Examples of pressure equalised mullions are presented in Figure 5. Because they have large webs, “arrow” or “rocket” shaped corner mullions of the sort shown in Figure 5-C, will experience pressure equalisation loads that are greater than those acting upon mullions in the flat areas of the same facade.

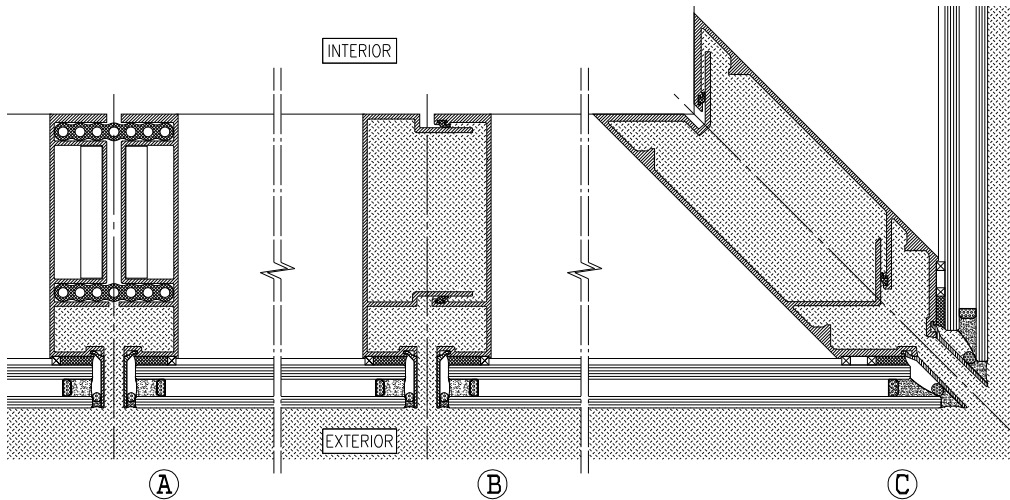


Figure 5: Inside pressure equalised mullions, wind pressure acts within the cavities that have been shaded and, consequently, forces act upon the webs and interior flanges.

If the air seal between the male and female sides is at the interior flange – this being the configuration in most unitised designs, and that shown in cases B



and C in Figure 5 – then the magnitude of the moment about the axis of extrusion,  $M_{z:p}$ , per unit length of member, is:

$$M_{z:p} = P \left( \frac{b}{2}(e_{sx} + (d_m - d_s)\theta_{z:p}) + d_m e_{sy} \right), \quad (3)$$

where  $P$  is the wind pressure at the exterior of the facade,  $b$  is the horizontal distance between mullions and  $d_m$  is the depth of the mullion in the direction perpendicular to the wall. Because the mullion profile's angle of rotation,  $\theta_{z:p}$ , must in reality be small,  $\theta_{z:p} \approx \sin \theta_{z:p}$ . The eccentricity between the shear centre and the load at the flange is  $e_{sx}$ , and the eccentricity for load at the web is  $e_{sy}$ . These dimensions are marked on the left hand mullion in Figure 6. The length  $(d_m - d_s)\theta_{z:p}$  is the amount by which the eccentricity between flange load and shear centre, shown in the sketch on the right hand side of Figure 4, changes as the mullion rotates. There is no corresponding adjustment for  $e_{sy}$  because the direction of the wind load is always perpendicular to the web, and there is no variation in eccentricity as the mullion rotates.

Strictly speaking, the pressure equalisation forces act upon the web in the region from the outer face of the front flange up to the air seal gasket at the interior flange, but, for simplicity, that distance is taken to be approximately equal to the mullion depth,  $d_m$ . Also, the moment obtained from Equation 3,  $M_{z:p}$ , is that acting at middle of the member's span, where rotation is greatest. In the analytical methods that follow, it will be assumed that  $M_{z:p}$  is applied uniformly over the whole length of the member. For design purposes, this assumption is on the safe side, but not excessively conservative: the axial torque is overstated in the zones away from the mid span, where the system's rotational response to moment is relatively small.

The moment due to pressure equalisation,  $M_{z:p}$ , causes the member to rotate about a longitudinal axis passing through the cross section's shear centre. In Figure 6, the left hand diagram shows, in solid line, the rotation of the cross section at the mid span, while the position of the cross section at the end of the span is shown in dashed line. The central diagram in Figure 6 shows the

lateral deflection caused by pressure equalization in the absence of  $M_{z:p}$ , and the right hand diagram shows the deflection occurring because of the combined effects of lateral bending and rotation about the longitudinal axis. Because of this combined deflection, the lateral movement of the members' outer flanges is small, making it possible to attach the extrusion to the glass using a flexible adhesive.

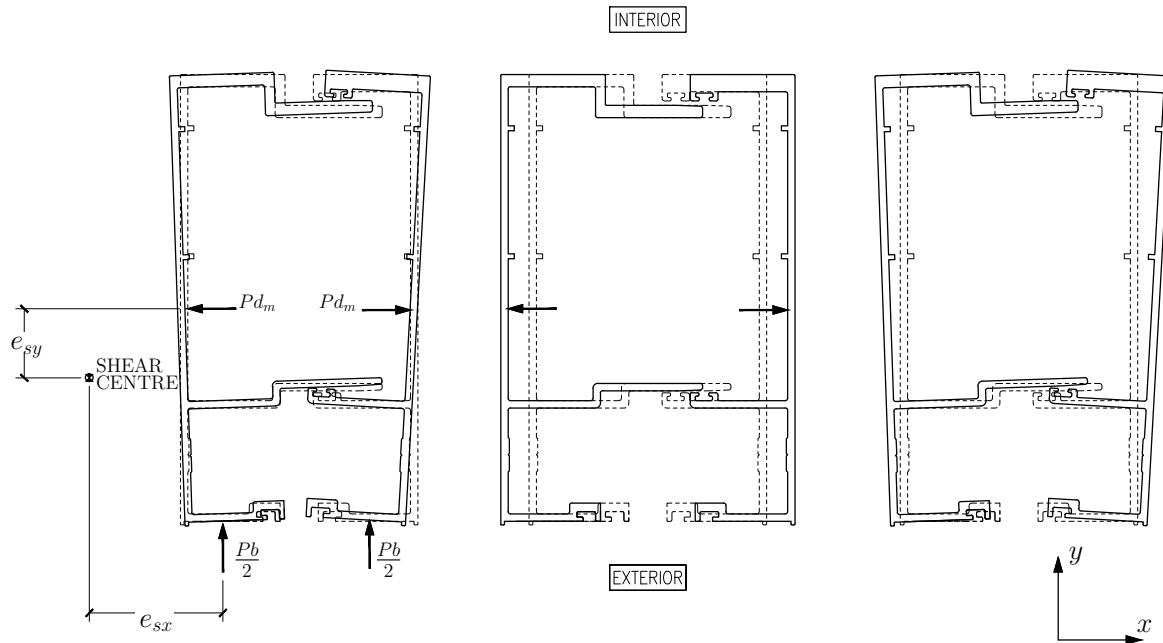


Figure 6: Plan view of mullions at mid-span (solid line) and at transom connections (dashed line), subjected to a moment about the longitudinal axis (left), subjected to a lateral load (centre) and subjected to a combined moment and lateral load (right).

Below, mullion rotation is considered in isolation. Lateral deflection is analysed separately, in Section 2.3.

A mullion extrusion is joined by its web to the transom members so that its cross-sectional profile can warp but not twist at these points of connection. If the torque applied about the member's axis is assumed to be uniformly distributed, as indicated in Figure 7, then the maximum rotation of the mullion profile,  $\theta_{z:p}$ , at the mid-point of the span between transoms, will be [24, p. 424, Table 10.3,

Case 2e];

$$\theta_{z:p} = \frac{M_{z:p}}{C_w E_a \beta^4} \left[ \frac{\beta^2 l_b^2}{8} + \frac{1}{\cosh\left(\frac{\beta l_b}{2}\right)} - 1 \right], \quad (4)$$

where  $M_{z:p}$  is the distributed torque (a moment per unit length of mullion),  $C_w$  is the profile's warping constant,  $l_b$  is the span between transoms, and;

$$\beta = \sqrt{\frac{J_{zz:m} G_a}{C_w E_a}}, \quad (5)$$

$J_{zz:m}$  being the profile's torsion constant and  $G_a$  being the shear modulus. For cross sections that are thin-walled and open, a method for calculating the warping constant,  $C_w$ , and also the location of the shear centre, is described by Xiang et al. [25]. The algorithm is intended for use in a computer program, but, with patience, it can be executed by hand [26]. An open source software package that makes use of finite element mesh methods to find the warping constant of open or boxed cross-sectional shapes, named *sectionproperties*, has been written by van Leeuwen [27].

Later, in Section 6.3, it is argued that, even if a structural sealant is used to bond the mullion's outer flange to the glass, the extrusion still will rotate about its shear centre. In this case, while the angle of rotation is small, the lateral or  $x$ -direction movement of a mullion extrusion's interior flange is;

$$\delta_{x:r} \approx d_s \theta_{z:p}. \quad (6)$$

### 2.3. Weak Axis Bending Due to Pressure Equalisation

The male and female profiles in a pressure equalised mullion both experience forces that cause rotation about the longitudinal axis, as considered in Section 2.2, and also bending about the weak axis, as shown in the central diagram in Figure 6. If the connections with transom members are moment resisting, then the deflection due to weak axis bending is easily calculated using

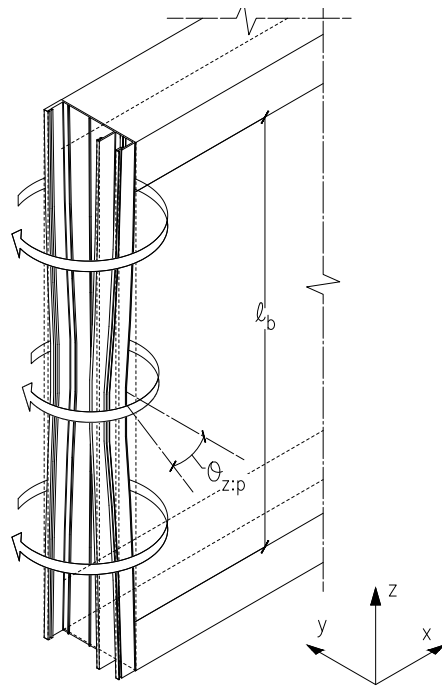


Figure 7: Uniformly distributed moment acting about the longitudinal axis of a mullion profile. At each end of the unbraced span, at the connections with transoms, the extrusion can warp but not twist.

the standard small-deflection beam formula [e.g. 24, Table 8.1, Case 2d]:

$$\delta_{x:b} = \frac{Pd_m l_b^4}{384E_a I_{yy:m}} \quad (7)$$

where  $l_b$  is the mullion's unrestrained span, which is the vertical distance between transoms, and  $I_{yy:m}$  is the mullion extrusion's second moment of area about its weak axis.

#### *2.4. Rotations at Edges of Glass Panes.*

If a gradually increasing pressure acts upon the surface of a glass pane, or on any other thin, edge-supported plate, then initially the induced stresses will be bending stresses, and deflection will vary in proportion to the applied load. As greater pressure is applied, membrane effects raise the apparent stiffness, and actual deflections will be less than those predicted by a model of bending alone. Even before the magnitude of deflection reaches the thickness of the plate, deviation from the linear load-deflection relationship can be appreciable [28, Fig. 7]. The large-deflection behaviour of a thin plate can however be found using a mathematical model that was first set out by Föppl [29] and, more famously, by von Kármán [30, p.350]. It is known that these differential equations do not take into account all of the stresses that occur in reality [31], but numerous studies [e.g., for glass, 32, p.65-74] have compared this model's predictions with the results of laboratory tests, or with the results of finite element analysis, with the finding that the analytical model is reliable over a wide range of conditions.

Navier worked on the theory of large deflection in plates [33, 34]. Applying a technique developed by his contemporary, Fourier, he considered the forces acting upon the plate to be the sum of a series of sinusoidally varying loads. He showed that, using this approach, it is possible find solutions to the Föppl and von Kármán system of differential equations. It is known that, under uniform lateral pressure, a pane of architectural glass whose four edges are attached to a supporting frame by conventional glazing gaskets or structural silicone sealant,

will behave as a simply supported plate [e.g. 35, p. 198]. A general solution for the deflection of a plate of this sort, obtained using Navier’s method, has been provided by Levy [28]. If its dimensions are  $a$  and  $b$  in the directions of the  $x$ -axis and  $y$ -axis respectively, then its deflection at a given point,  $w(x, y)$ , will be [28, Equation 6]:

$$w(x, y) = \sum_{m=1,2,3\dots}^{\infty} \sum_{n=1,2,3\dots}^{\infty} w_{m,n} \sin\left(\frac{m\pi x}{a}\right) \sin\left(\frac{n\pi y}{b}\right). \quad (8)$$

The effort required to determine the  $w_{m,n}$  coefficients is not insignificant, but, since the series converges quickly, a useful approximation can be obtained by considering only the term containing  $w_{1,1}$ . So, Equation 8 can be rewritten:

$$w(x, y) \approx w_{1,1} \sin\left(\frac{\pi x}{a}\right) \sin\left(\frac{\pi y}{b}\right). \quad (9)$$

In the present discussion of rotational influences on mullions, it is approximate scale, rather than the precise values, that are of interest. In this context, the accuracy of the above expression is adequate. For example, for a square plate with Poisson’s ratio of 0.316, at values of  $Pa^4/Eh^4$  above 150,  $w_{1,1}$  is greater than the exact central deflection by only 9% [28, Fig. 7].

Measured along any line that is parallel to a side of the plate, the out-of-plane deflected shape is one half period of a sinusoid, as shown in Figure 8. The slope of the deflected glass can be found by partial differentiation of Equation 9. If a glass pane is orientated so that the side with length  $a$  is vertical, and it is viewed in plan, then the gradient of the glass with respect to its normal plane is:

$$\frac{\partial w}{\partial y} \approx \frac{\pi w_{1,1}}{b} \sin\left(\frac{\pi x}{a}\right) \cos\left(\frac{\pi y}{b}\right). \quad (10)$$

The deflection of architectural glass is commonly limited to 1/60 of the plate’s shorter dimension [e.g 36, Section 3.3.3]. Substituting  $b/60$  for  $w_{1,1}$  in Equation 10, and converting the gradient to an angle of rotation,  $\theta_{z:g}$ , in radians:

$$\theta_{z:g} \approx \arctan \left[ \frac{\pi}{60} \sin \left( \frac{\pi x}{a} \right) \cos \left( \frac{\pi y}{b} \right) \right]. \quad (11)$$

At the glass edge that is in contact with the mullion, the angle of rotation of the glass is greatest at the mid-point between transoms, where  $x = a/2$  and  $y = b$ . Hence, all of the foregoing plate analysis leads to the simple but important result that, when full design pressure is applied, the maximum angle through which the edge of an architectural glass pane will rotate is approximately 0.0523 radians or 3 degrees. This figure is used in the models that follow.

### 2.5. Moments Transferred Through Structural Silicone Sealant

When glazing a prefabricated curtain wall panel, it is now the usual practice to bond the glass to the outer flange of the aluminium framing members using structural silicone sealant. Examples of these adhesive joints can be seen in Figures 3 and 5, and a brief history of structural sealants, with guidelines for

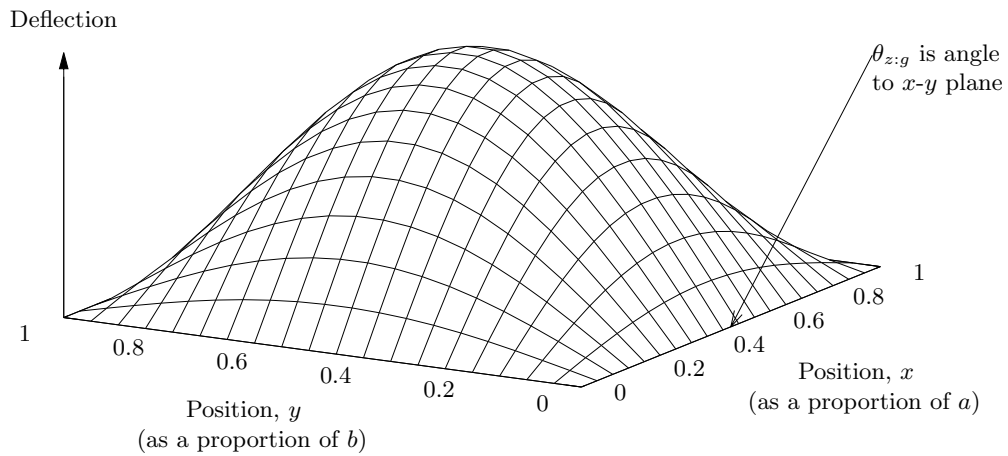


Figure 8: Sinusoidal deflection of a pane of glass, described by Equation 9.

usage and stress analysis, may be found in ASTM C1401 [37].

In a previous study [38, Equation 4], the relationship between the angle of rotation at the edge of the glass,  $\theta_{z:g}$ , and the axial moment that is transferred to the mullion,  $M_{z:s}$ , was proposed to be;

$$M_{z:s} = \theta_{z:g} \frac{B^3 E_s}{12g}, \quad (12)$$

this angle being in radians, while  $B$  and  $g$  are the sealant joint's cross-sectional dimensions – its bite and glueline – measured, respectively, in the directions parallel and perpendicular to the glass. A linear elastic response is assumed, and  $E_s$  is the Young's modulus of the sealant.

Figure 9 shows the transfer of moment from the curtain wall's face or infill material, which is typically glass, through the structural silicone joint, to the exterior flange of the mullion.

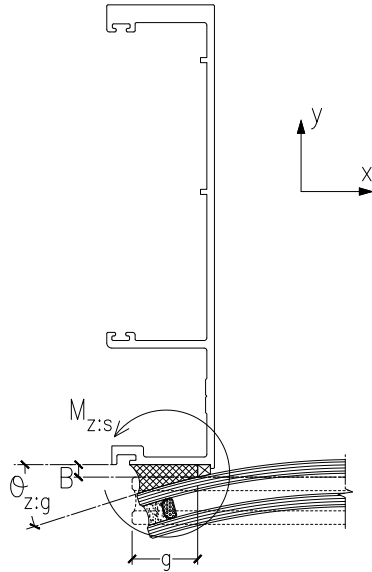


Figure 9: Acted upon by wind pressure, glass edges rotate, and a moment is transferred through the structural sealant to the mullion extrusion.

Typical published values of  $E_s$  are between 1 and 2 MPa [e.g 39]. However,



laboratory tests carried out during the same past study suggested that the apparent value of Young's modulus increases with  $B$  [38, Section 7.2]. The test data indicate that, for a real structural silicone connection, the value of  $M_{z:s}$  might lie somewhere between one and two times the value found using Equation 12.

### 2.6. Asymmetric Bending

If a mullion profile's principal axes – the two centroidal axes about which it is strongest and weakest – are not parallel to its webs and flanges, then, even if load is applied only in the direction normal to the wall, there will be a component of displacement parallel to the wall. In Figure 10,  $x'$  and  $y'$  are the principal axes of a female extrusion, and the angle that they make with the  $x$ – and  $y$ –axes, which are parallel to the profile's flanges and webs respectively, is  $\alpha$ , where [25, Equation 7];

$$\alpha = \frac{1}{2} \operatorname{atan} \left( \frac{2I_{xy}}{-I_{xx} + I_{yy}} \right), \quad (13)$$

and the section's second moments of area about its principal axes are;

$$I'_{xx} = \frac{I_{xx} + I_{yy}}{2} + \sqrt{I_{xy}^2 + \frac{(I_{xx} - I_{yy})^2}{4}}, \quad I'_{yy} = \frac{I_{xx} + I_{yy}}{2} - \sqrt{I_{xy}^2 + \frac{(I_{xx} - I_{yy})^2}{4}}. \quad (14)$$

For a given curtain wall panel, deflection in the direction perpendicular to the wall,  $\delta_x$ , measured with respect to the transoms at the ends of the unbraced span, varies directly with wind load, so, for convenience in the analysis that follows, a temporary constant,  $k$  is introduced;

$$k = \frac{I_{xx}q}{\delta_x}, \quad (15)$$

where  $q$  is the force per unit length of member.

Analysing the movement of an asymmetric extrusion at a single unbraced span, as on the right hand side of Figure 10, is complicated. The process be-

gins with the vector decomposition of the direct load,  $q$ , and also the moments,  $M_1$  and  $M_2$ , into components aligned with the principal axes. The mullion's responses in the directions parallel and perpendicular to the wall are affected by the different support conditions in the two planes. For bending in the plane of the wall, the ends of the mullion's span are fixed to the transoms and these connections are moment-resisting. At the same time, for bending in the plane perpendicular to the wall, the transoms offer no moment resistance. For simplicity in this current analysis, the in-plane moment resistance of the horizontal members will be ignored. Therefore, the in-plane flange movements predicted using Equation 18, below, will be overestimates, possibly gross overestimates, but they will be useful nonetheless.

Decomposing the loads into vector components parallel to the principal axes;

$$q \sin(\alpha) > \frac{k\delta'_y}{I'_{yy}}, \quad q \cos \alpha > \frac{k\delta'_x}{I'_{xx}}, \quad (16)$$

and then taking the components of displacement in the direction parallel to the wall;

$$\delta_{x:a} < k_{mf}(\delta'_y \cos \alpha - \delta'_x \sin \alpha). \quad (17)$$

Replacing the terms in Equation 17 with the expressions given in Equations 13, 14, 15 and 16;

$$\delta_{x:a} < \frac{\delta_x k_{mf}}{I_{xx}} \sqrt{I_{xy}^2 + \frac{(I_{xx} - I_{yy})^2}{4}} \sin \left( \text{atan} \left( \frac{2I_{xy}}{I_{xx} - I_{yy}} \right) \right) \quad (18)$$

So that the polarity of deflection will be positive when the extrusion flanges move away from the mullion's centreline,  $k_{mf} = -1$  when the profile, usually male, is on the left hand side when the split mullion is viewed from the exterior of the building, and  $k_{mf} = 1$  for the other profile.

### 2.7. Rotation at Ends of Transoms

It is conservative to assume that, in the direction perpendicular to the wall, the load acting upon a transom is uniformly distributed and is caused by the

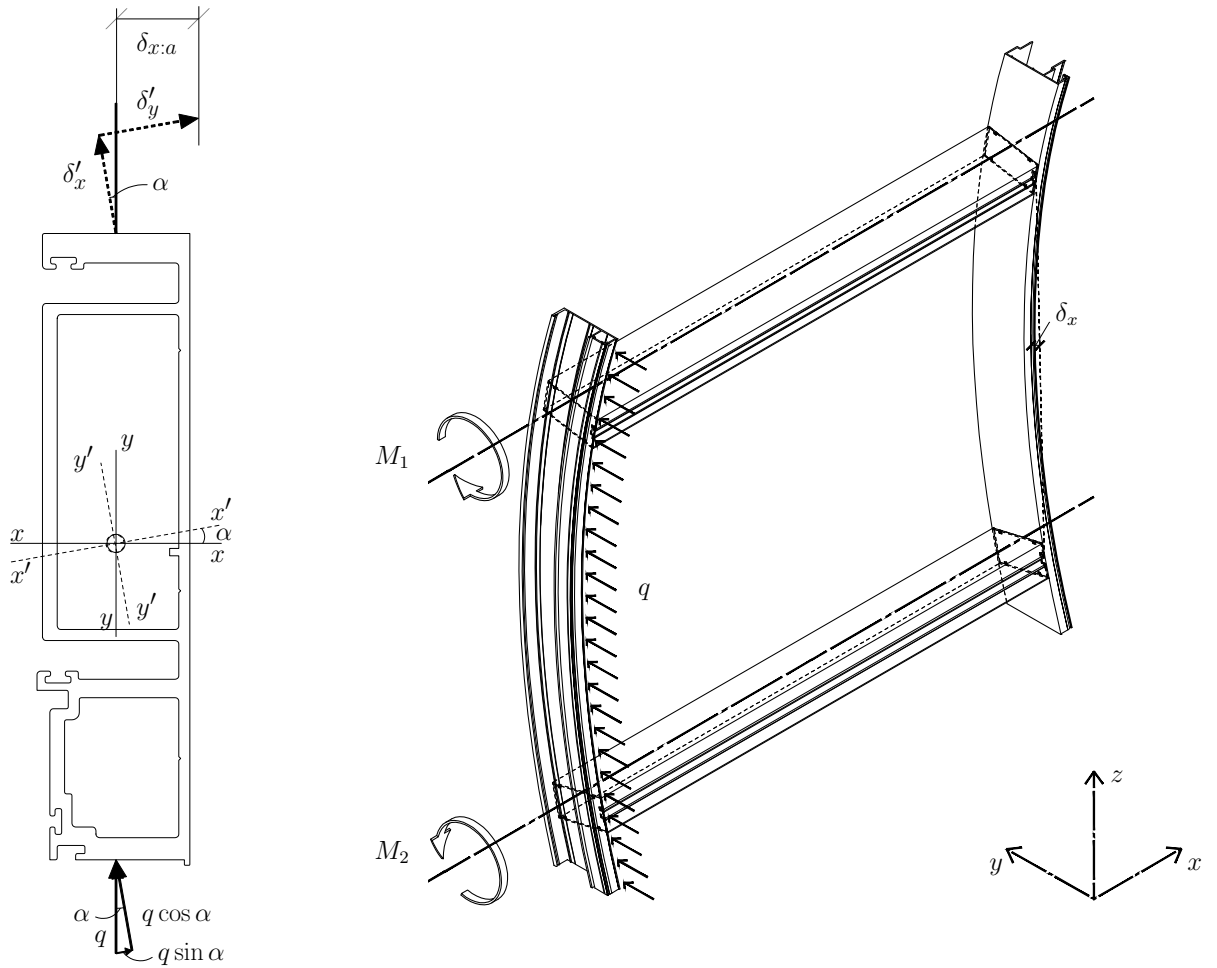


Figure 10: Vector components of load, in solid line at exterior flange, and components of deflection, in dotted line at interior flange, in female mullion extrusion (left) with principal axes  $x'$  and  $y'$ . Deflection of the mullion at one unbraced span in a unitised curtain wall panel (right).

action of wind upon a tributary strip whose height is equal to the transom length,  $b - b_m$ . Such a transom is shown in Figure 11. The deflection of the member is of interest because, at each end, it is rigidly connected to the web of a mullion, and so transom flexure causes the mullion profiles to rotate about their longitudinal axes. If it is assumed that the mullion is weak in torsion, so that it does not resist rotation of the transom's ends, then the angle of rotation  $\theta_t$  radians, can then be found using the standard formula for a simply supported beam [24, p. 193, Table 8.1, Case 2e]:

$$\theta_t = \frac{P(b - b_m)^4}{24E_a I_{xx:t}}, \quad (19)$$

where  $I_{xx:t}$  is the transom's second moment of area about a vertical axis through its centroid.

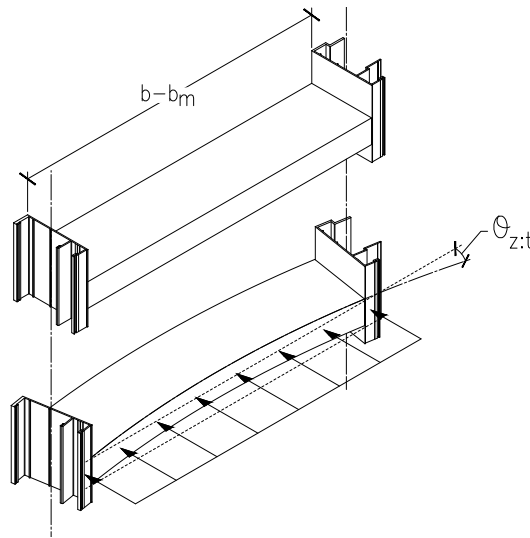


Figure 11: When transom member goes from the unloaded (upper sketch) to loaded condition (lower sketch), flexure causes the attached mullion profiles to rotate about their longitudinal axes.

### 2.8. In-plane-of-wall Movement of Glass Edge

When wind load causes a pane of architectural glass to deflect, the edges of the pane move in the plane of the wall. If the glass is bonded to its structural

frame, then movements at its edges will cause the mullions to rotate. The approximate glass deflection model described in Section 2.4 is considered again in this present discussion, but now, as shown in Figure 12, the  $y$ -axis has been aligned with the centre of the plate. The deflected shape of the pane, measured in a horizontal plane passing through its geometric centre, is a cosine with amplitude  $w_{max}$ .

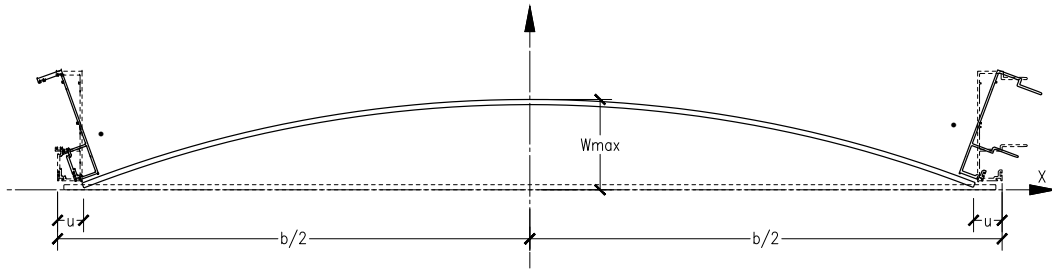


Figure 12: When wind pressure causes a glass pane to deflect, its edges move in the plane of the wall, and the mullion profile rotates.

Working from first principles, it is not difficult to develop an integral for the arc length of the curve, which is equal to the original width of the flat pane,  $b$ . If the in-plane movement of a glass edge is  $u$  then:

$$b = \int_{-(\frac{b}{2}-u)}^{\frac{b}{2}-u} \sqrt{1 + \left( \frac{d}{dx} \left[ w_{max} \cos \left( \frac{\pi x}{b - 2a} \right) \right] \right)^2} dx \quad (20)$$

An expression of this form, an elliptic integral, has no closed-form solution. However, with the assumption that was introduced in Section 2.4, that the maximum glass deflection in the direction normal to the plane of the wall,  $w_{max}$ , is  $b/60$ , then numerical evaluation reveals that  $u$  is, at most,  $b/2918$ .

### 3. Example Unitised Curtain Wall

The shapes and structural properties of a male and female mullion pair are shown in Figures 14 and 15, and the geometry of the facade in which they are used is shown in Figure 13. The lateral movements of this curtain wall

system's mullion profiles have been modelled numerically and algebraically, as described in Sections 4 and 5. In these studies, it is assumed that the profiles are extruded in 6063 aluminium alloy, and that the temper is T5. The vertical dimensions given in Figure 13 are measured from the fulcrums of the stack joints and brackets.

For the purpose of determining the magnitude of the bending moment acting about the mullion's x-axis, the load upon each mullion is considered to act only in the direction perpendicular to the wall, and to be uniformly distributed, without any concentration of load at the points of connection with transoms. These assumptions are consistent with the example given in the ADM [11, Part VIII, Figure 28d, p. 60]. Stresses caused by axial loads, which are small in comparison with flexural stresses, are ignored.

Theoretical bending moments, shear forces and deflections in mullions, at the design load of 4.6 kPa, are shown in Figure 16. These theoretical curves follow from the classical theory of small deflections in elastic beams, and have been determined numerically, using an open source frame analysis software package, Frame3DD [40].

In this wall system, which complies with the ADM's structural design rules, the limiting structural design constraint is LTB resistance.

#### **4. Numerical Simulation Using Code Aster and Salome-Meca**

An open-source finite element software package, Code Aster [41], and a compatible pre- and post-processing environment named Salome-Meca [42], have been used to simulate the shape changes that occur when load is applied to the split mullion in the curtain wall specimen shown in Figures 13. Finite element meshes representing the glass, sealant and aluminium profiles in two horizontally-adjacent panels were studied. In order to avoid unnecessary computation, each panel was divided at its vertical centreline, and only one half was included in the model. The pair of adjacent half-panels is pictured in Figure 17.

The model's boundary conditions were set to mimic the restraint provided

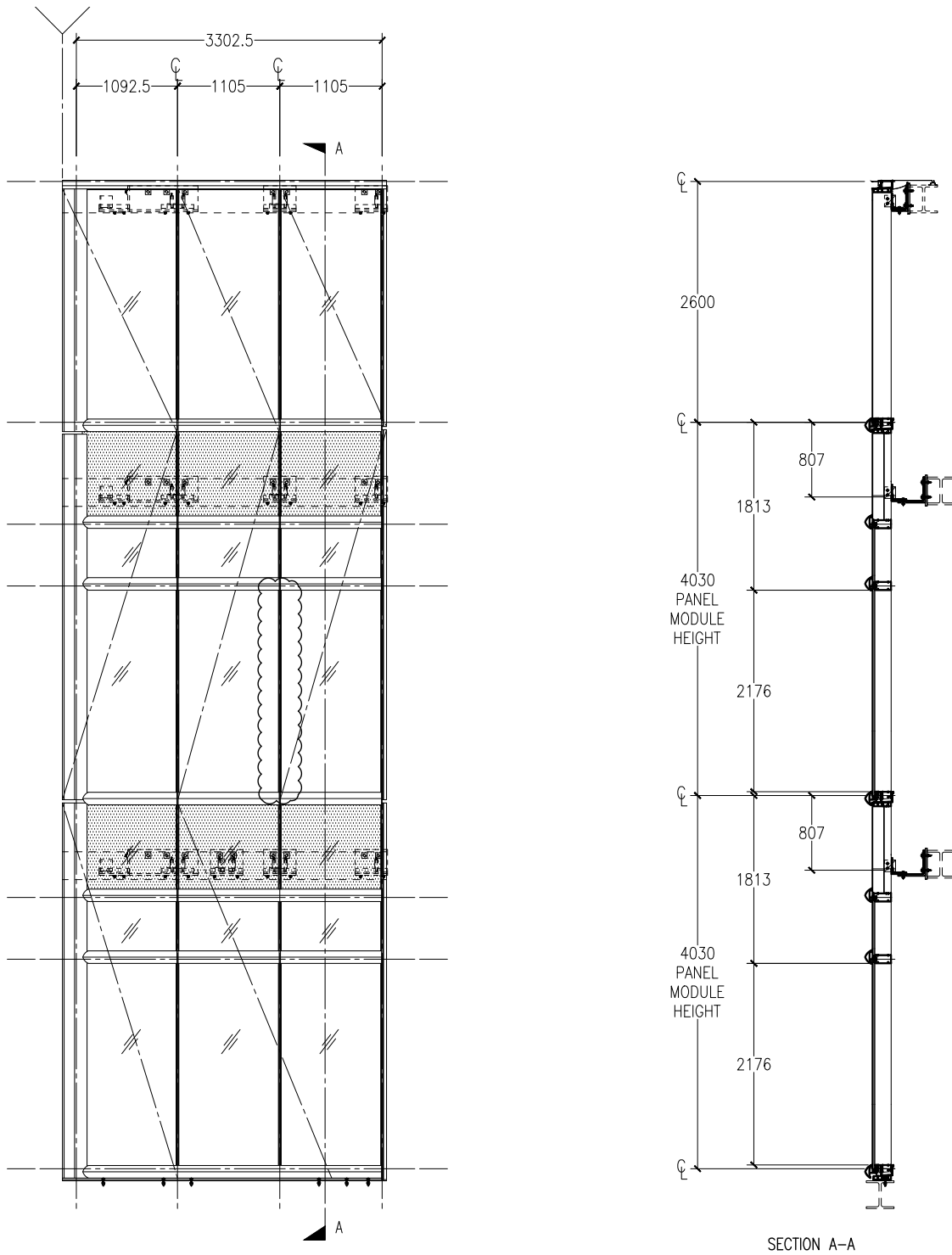
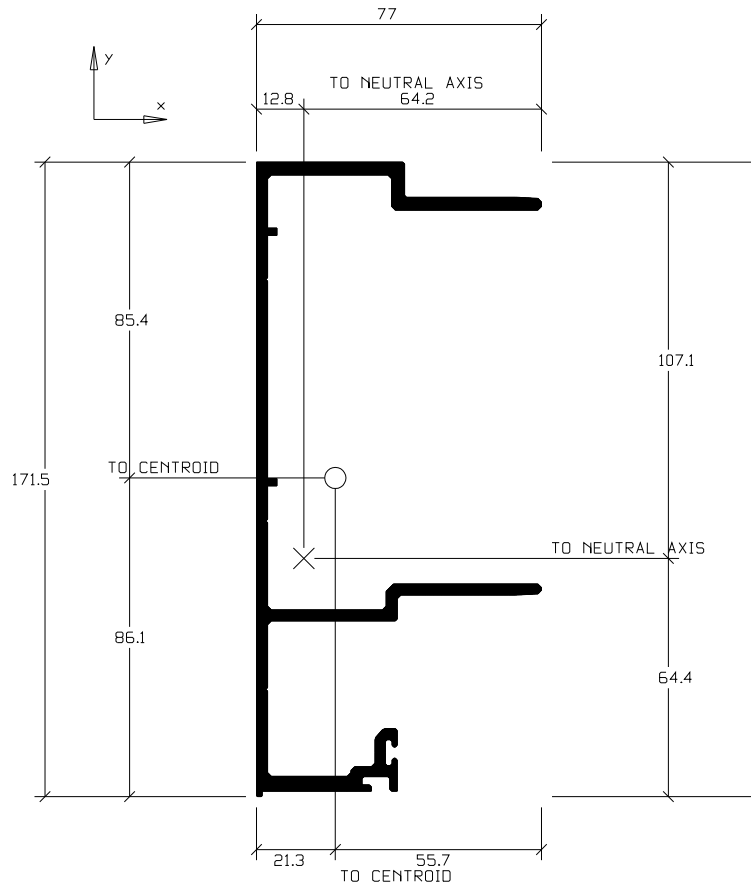


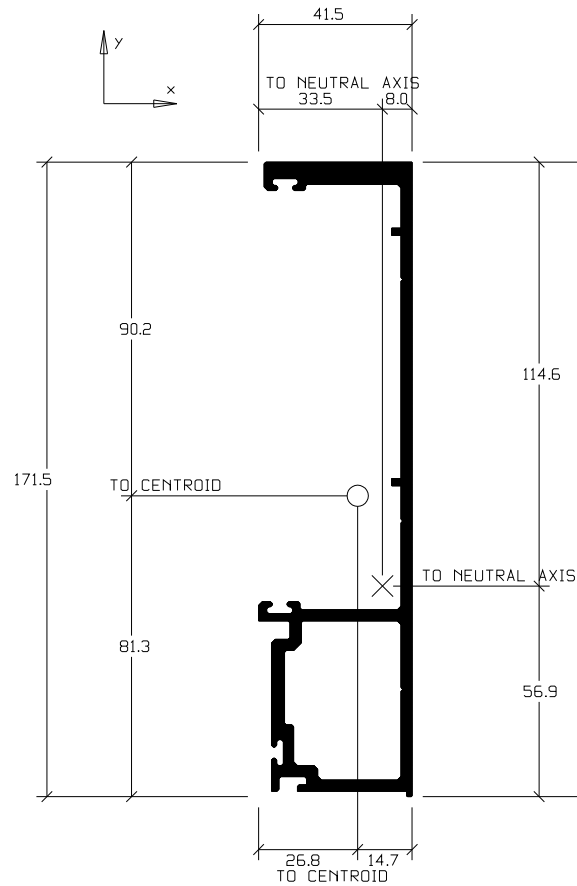
Figure 13: Exterior elevation and section view of curtain wall considered in analytical and finite element studies. The mullion span considered in this study is shown within the 'cloud'.



Cross sectional area:	1243.3	mm <sup>2</sup>
Overall section width (in $x$ direction):	77.0	mm
Overall section depth (in $y$ direction):	171.5	mm
$x$ -coordinate of shear centre with respect to centroid:	-43.71	mm
$y$ -coordinate of shear centre with respect to centroid:	14.41	mm
Radius of gyration about centroidal $x$ -axis:	60.59	mm
Radius of gyration about centroidal $y$ -axis:	22.15	mm
Second moment of area about centroidal $x$ -axis, $I_{x:m}$ :	$4.558 \times 10^6$	mm <sup>4</sup>
Second moment of area about centroidal $y$ -axis, $I_{y:m}$ :	$0.619 \times 10^6$	mm <sup>4</sup>
Product moment of area, $I_{xy:m}$ :	$0.224 \times 10^6$	mm <sup>4</sup>
Torsion constant, $J_{z:m}$ [3, Part II, Chapter B.1]:	$4.167 \times 10^3$	mm <sup>4</sup>
Warping constant, $C_w$ :	$2.56 \times 10^9$	mm <sup>6</sup>

Figure 14: Structural section properties of the male mullion profile in the wall specimen shown in Figure 13.





Cross sectional area:	1151.6	mm <sup>2</sup>
Overall section width (in $x$ direction):	41.5	mm
Overall section depth (in $y$ direction):	171.5	mm
$x$ -coordinate of shear centre with respect to centroid:	23.79	mm
$y$ -coordinate of shear centre with respect to centroid:	-6.60	mm
Radius of gyration about centroidal $x$ -axis:	51.33	mm
Radius of gyration about centroidal $y$ -axis:	14.30	mm
Second moment of area about centroidal $x$ -axis, $I_{x:m}$ :	$4.334 \times 10^6$	mm <sup>4</sup>
Second moment of area about centroidal $y$ -axis, $I_{y:m}$ :	$0.237 \times 10^6$	mm <sup>4</sup>
Product moment of area, $I_{yx:m}$ :	$0.182 \times 10^6$	mm <sup>4</sup>
Torsion constant, $J_{zz}$ [3, Part II, Chapter B.1]:	$195.99 \times 10^3$	mm <sup>4</sup>
Warping constant, $C_w$ :	$0.942 \times 10^9$	mm <sup>6</sup>

Figure 15: Structural section properties of the female mullion profile in the wall system shown in Figure 13.

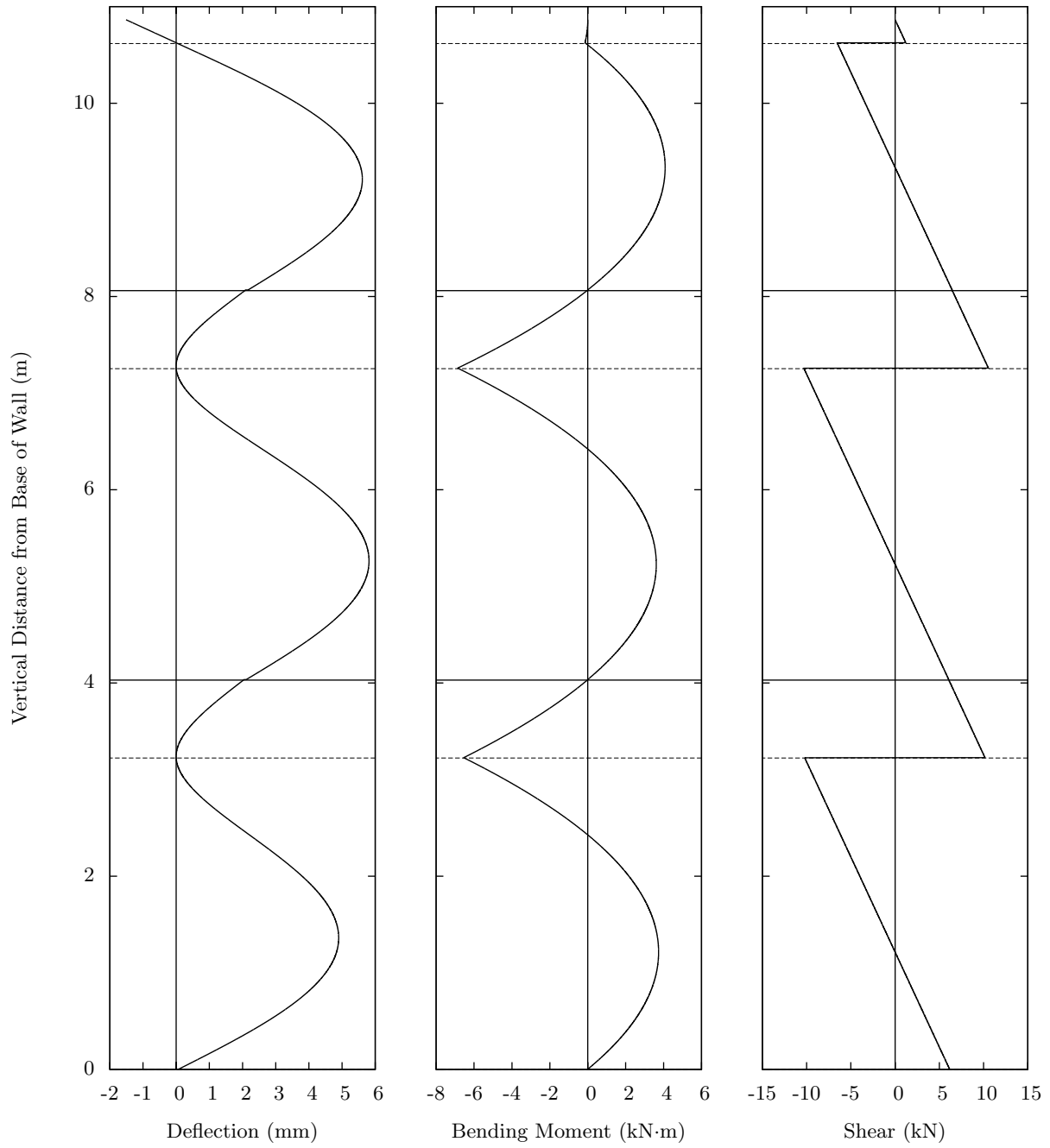


Figure 16: Theoretical deflection, bending moment and shear in the curtain wall specimen's mullions at 4.6 kPa. In these graphs, the locations of brackets are marked by dashed vertical lines: continuous vertical lines show the positions of stack joints.

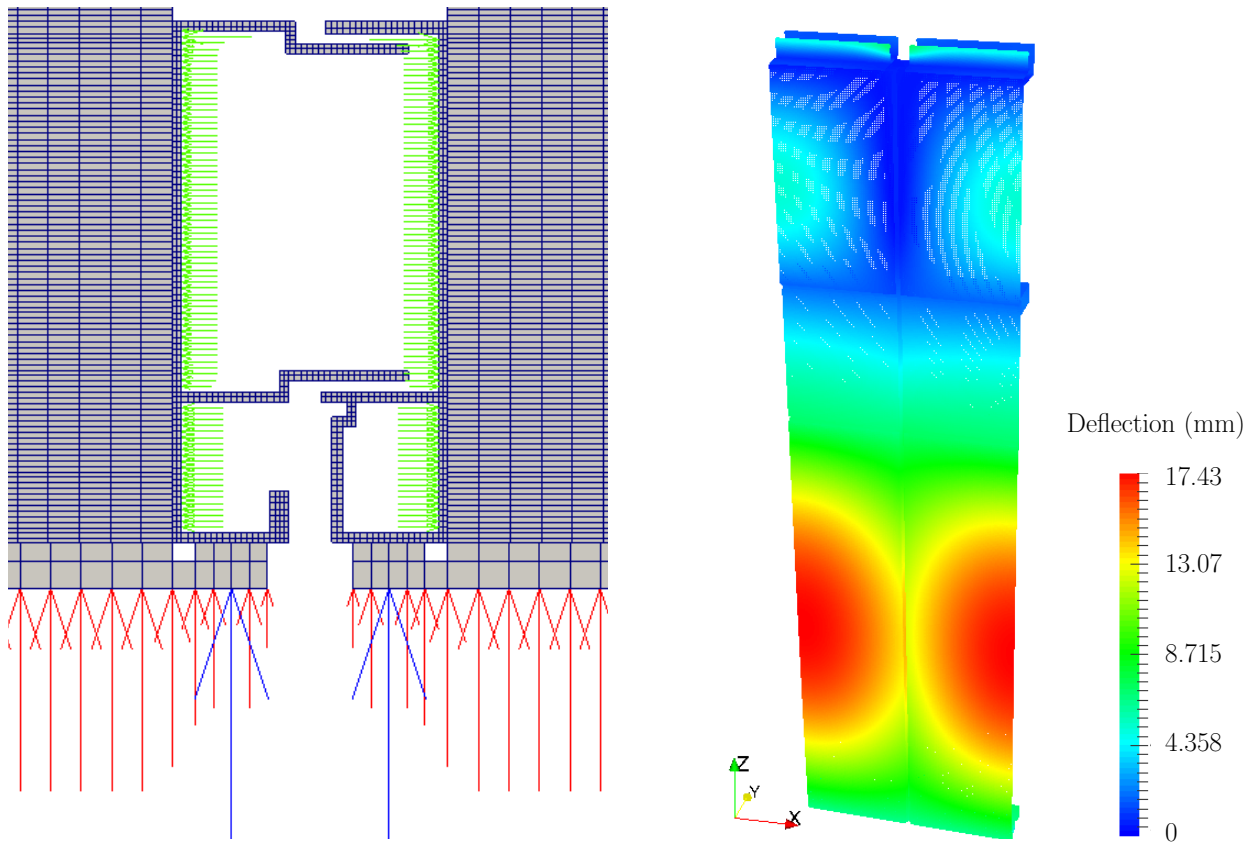


Figure 17: Loads considered in the finite element model (left), and the deflected shape of the two adjacent half-width panels (right).

by the missing half-panels, as well as the loads from panels above and below. In this way, each half-panel in the model is forced to behave as if it were part of a normal, multi-floor curtain wall.

The Young's modulus of the structural silicone sealant is taken to be 1.1 MPa, which is the value published by the manufacturer of the product (DC-983) used in the laboratory test specimens [39]. This material is, in reality, visco-elastic, but providing strains are not extreme, in this practical context it is reasonable to assume a linear elastic response [38, p. 512]. Rubber gaskets that are present in the real curtain wall system, at the joints between the male and female mullion profiles, visible in Figure 5-B, have not been included in this computer simulation. The coefficient of friction between the metal surfaces has been taken to be zero.

Only the inner pane of the insulated glass unit, or IGU, has been modelled in full. This pane carries a pressure equal to  $(t_i^3 + t_e^3)P/t_i^3$ , where  $t_i$  and  $t_e$  are the thicknesses of the IGU's inner and outer panes, and  $P$  is the total wind load acting upon the facade. This load share formula is consistent with design codes for structural analysis of architectural glass, such as ASTM E1300 [43, Appendix X3]. The component of wind pressure acting upon the outer pane has been modelled as a line load at the center of the structural silicone connection to the mullion's outer flange. In addition to the wind pressure on the glass, the same pressure has been considered to act within the mullion's internal cavities, as indicated in Figure 5-B. The forces are shown diagrammatically in Figure 17: pressure acting upon the inner pane of the insulated glass unit is indicated in color red, the load transferred from the outer pane is in blue, and wind pressure in the direction parallel to the wall, upon each extrusion's web, is shown in green.

For each load case, displacements were calculated iteratively until the forces at each node, in the directions parallel to the axes, had converged to an equilibrium state, with a tolerance of  $1 \times 10^{-6}$  N. The effect of varying the mesh density was investigated, and it was found that changing from the model shown in Figure 17 to that shown in Figure 18 had little influence upon the deflected

shape predictions. The values indicated in this paper have been obtained from a model with approximately 700,000 nodes.

The deflected shapes of the male and female mullion extrusions, from the curtain wall specimen shown in Figure 13, at the middle of their longest unsupported span, are drawn in bold color in Figure 18; in the same image the positions of the components in their unloaded conditions are shown in outline.

The FEA models have yet to be validated by physical testing. However, the software – which is made up of 1.5 million lines of source code, accompanied by 14,000 pages of technical documentation and more than 3,600 standardized test cases – is known to be mature, and is believed to be reliable: it has been developed continuously since 1980 by the French state’s electrical power conglomerate, EDF, and has been widely used in the design of nuclear power facilities [41].

## **5. Relative Importance of Factors Causing Mullion Twist**

Contributions to the lateral movements of the interior flanges of the mullion profiles in the curtain wall system described in Section 3, and moments acting about the extrusions’ longitudinal axes, have been calculated using the expression introduced in Section 2.

The results, set out in Table 1, demonstrate that the rotational moment attributable to the phenomena that are collectively termed lateral torsional buckling is, for practical purposes, negligible in comparison with the moments that are attributable to the eccentricity between the shear centre and the applied wind loads. Similarly, it is reasonable to ignore rotations due to the transom’s flexure, and the mullion rotations caused by movements of the glass edges in the plane of the wall, and the lateral movement associated with asymmetric bending. Inspection of the algebraic expressions suggests that, for the facade layouts and design pressures encountered in real buildings, these findings will apply to all of the unitised curtain wall systems in which air seals are located at the mullion’s interior flange.

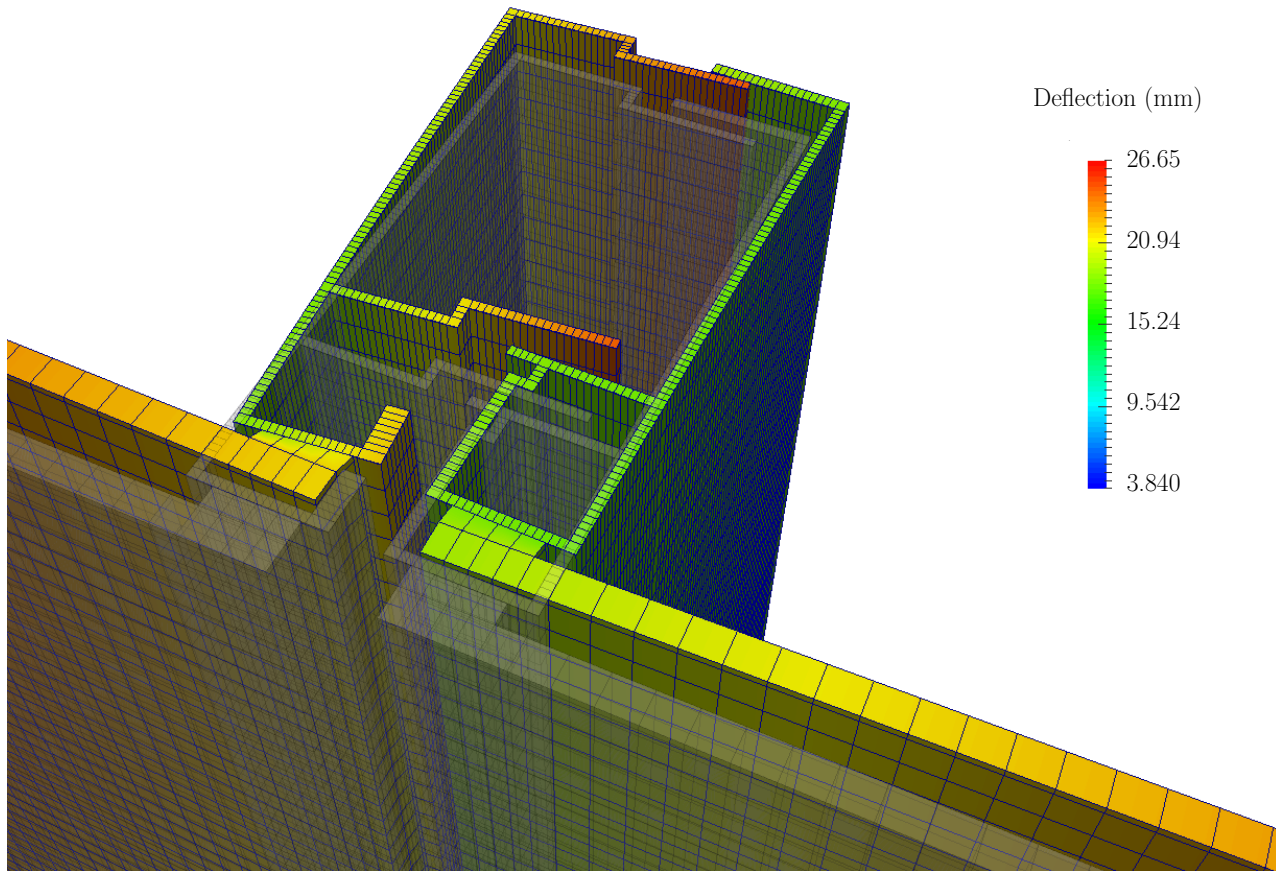
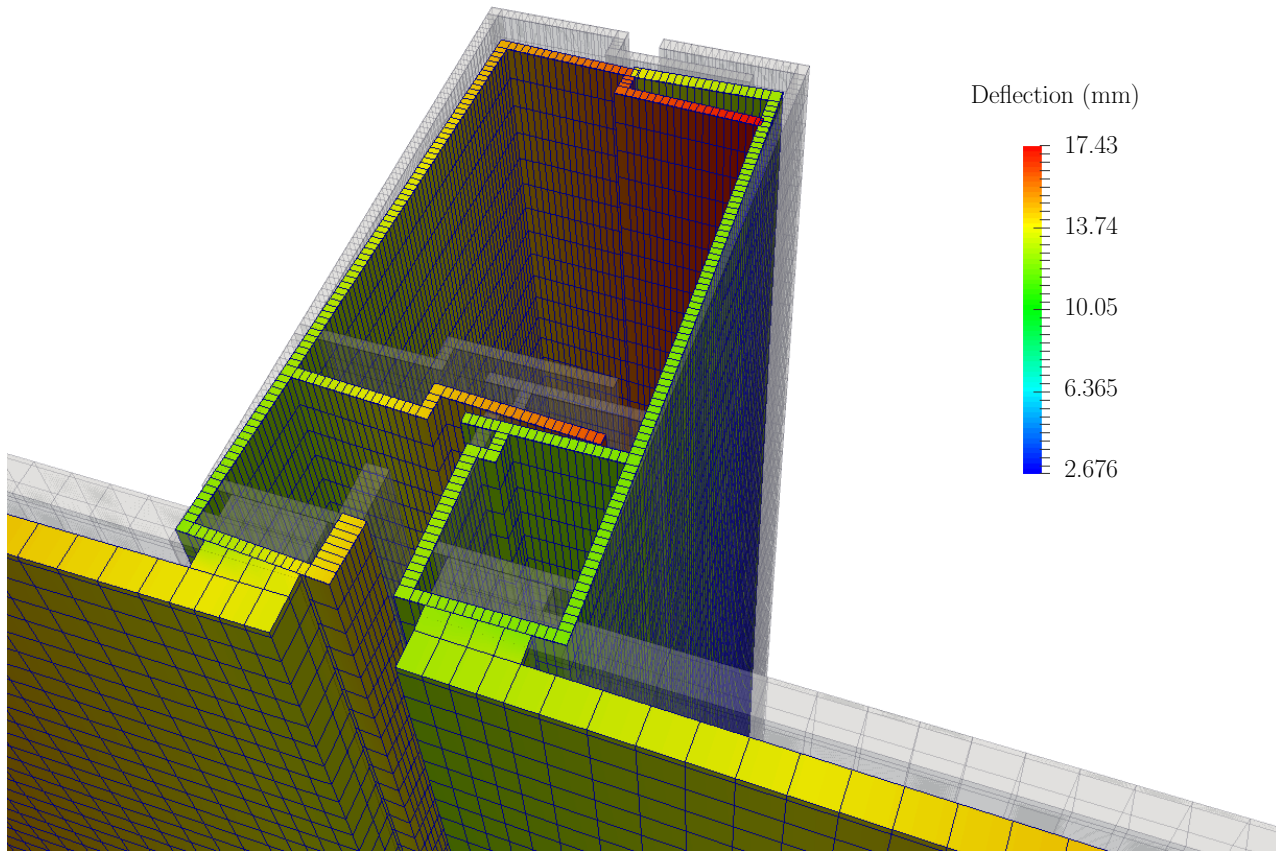
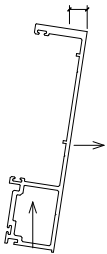

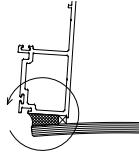
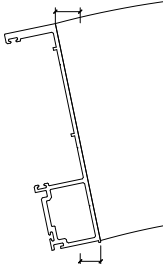
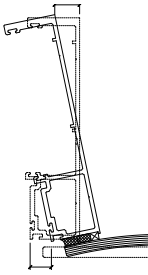


Figure 18: The deflected positions of the mullion profiles at wind pressures of -4.6 kPa (upper diagram), and +6.75 kPa (lower diagram). The components' unloaded positions are shown in outline.

Table 1: Contributions of different physical effects to the moments in, and lateral displacement of, interior flanges of mullion profiles in the curtain wall described in Section 3, at a wind pressure of 4.6 kPa.

Phenomenon	Axial Moment (N.mm/mm)		Lateral Disp. of Int. Flange (mm)		Diagram	Notes
	Male	Female	Male	Female		
a Lateral torsional buckling.	< 0.807	< 1.89	–	–	See Figure 2.	See Equation 2. Magnitude is small in comparison with effects in rows b and c below.
b Rotation caused by wind loads on flanges and webs.	132.9	73.0	11.9	0.803		See Equations 3, 4 and 5.
c Deflection in plane of wall caused by pressure equalisation.	–	–	1.07	2.80		See Equation 7.
d Asymmetric bending.	–	–	< -0.145	< 0.124	See Figure 10	See Equation 18; $\delta_x$ from Figure 16.
e Moment transmitted through structural silicone sealant.	-17.5	-13.2	–	–		See Equation 12. Values are maxima, occurring at the mid span. Glass rotation is 3°, and mullion rotations are from FEA (see Table 2).
f Rotation of transom end.	–	–	-0.112	-0.112		See Equation 19. Reasonably, this effect can be ignored.
g Mullion rotation caused by glass edge movement in plane of wall.	–	–	-0.267	-0.491		See Equation 20. Reasonably, this effect can be ignored.

The lateral movement occurring at the mid span of the interior flange of a mullion profile can therefore be estimated by summing both the rotation caused by moments about the longitudinal axis together with the weak-axis bending that is the result of pressure equalisation. These are the two effects described in Sections 2.2 and 2.3. An expression for the magnitude of this deflection in the plane of the wall can be obtained by combining Equations 3, 4, 5, 6 and 7. If  $\delta_{x:s}$  is the total horizontal movement of the flange of a mullion profile, in the plane of the wall, then;

$$\delta_{x:s} \approx \frac{Pd_m l_b^4}{384E_a I_{yy:m}} + \frac{d_s P (b e_{sx} + 2d_m e_{sy}) (k_1 - l_b^2 k_2)}{bP(d_m - d_s)(l_b^2 k_2 - k_1) - 16G_a J_{zz:m} k_2}, \quad (21)$$

where;

$$k_1 = 8C_w E_a \left( e^{\frac{1}{2} l_b \sqrt{\frac{G_a J_{zz:m}}{C_w E_a}}} - 1 \right)^2, \quad (22)$$

and;

$$k_2 = G_a J_{zz:m} \left( e^{l_b \sqrt{\frac{G_a J_{zz:m}}{C_w E_a}}} + 1 \right). \quad (23)$$

Equation 21 applies to the split mullion members in a unitised curtain wall whose air seal is located at the profiles' interior flanges.

## 6. Discussions

Arguments regarding the validity of the algebraic models that are the basis for the flange movement predictions summarized in Table 1, are set out below, together with comments on the level of agreement between the analytical and finite element simulations.

### 6.1. Pressure Equalization

The principle of pressure equalisation is one that is encountered regularly in the facade industry. The role that it plays in weatherproofing is usually one of the first topics to be covered in curtain wall design textbooks and training courses, and it is frequently mentioned in technical specifications. Therefore, at least in the context of controlling water entry, the concept is familiar to every



facade engineer. Given this high level of awareness, it is odd that the structural consequences of pressure equalisation – the loads that it places upon a mullion’s webs – are not even mentioned in the existing literature, nor have the authors ever seen structural calculations in which it is taken into account.

This paper’s analytical methods, which consider the loads acting upon mullion webs, therefore are novel.

### *6.2. Twisting Moment Due to LTB*

Torsional bracing can be used to prevent lateral torsional buckling of a slender flexural member, and the moment transferred to such a brace will be less than the estimate obtained using Equation 2. However, in the derivation of this expression, it is assumed that the member’s cross section has at least one axis of symmetry, whereas, in reality, there is no line of symmetry in a unitised mullion profile. Therefore, the explanation in the following paragraph is required to justify the use of this analytical method with unitised mullion extrusions, which are invariably asymmetric.

The moment that causes a mullion profile to rotate about its longitudinal axis can be divided into two components. One part, the eccentric loading moment, is induced by applied loads whose line of action does not pass through the cross section’s shear centre. The other part is attributable to the various buckling effects outlined in Section 2.1, whose total is known to be less than the moment found with Equation 2. So, if the sum of buckling moments can be shown to be small in comparison with the eccentric loading moment – which will normally, perhaps always, be the case for unitised mullions – and if it can be shown that the profile’s torsional rigidity is such that the eccentric loading moment causes only slight rotation, then it follows that the design is resistant to lateral torsional instability. Expressed another way, if the buckling moment from Equation 2 is small in comparison with the eccentric loading moment from Equation 3, and if Equations 21 to 23 show that lateral movements of flanges will be small, then further analysis of LTB is unnecessary.

### *6.3. Rotation About Shear Centre*

When a moment is applied about the longitudinal axis of a prismatic member that is held only at its ends, as in Figure 7, the cross section will rotate about its shear centre. However, the members considered in this study are not completely free to rotate in this way, as they are attached by structural sealant to a face or infill material that is often glass, and it is therefore reasonable to ask whether the member in fact rotates about the centre of the sealant connection. The explanation that follows will therefore be helpful.

In the analytical models established in Section 2, it has been assumed that rotation occurs about the shear centre. Such rotation cannot occur freely on its own because the mullion's outer flange is bonded to the glass. However, as well as rotating, the member is also deflecting about its weak axis, and when bending and rotation occur together, the relative movement between the outer flange and the glass is much smaller than the movement that would be caused by bending or rotation alone. This combination of effects may be seen in Figure 6. The sealant is an elastomer with a low modulus of elasticity, and it is capable of accommodating lateral movements that are comparable with, or greater than, the sealant joint thickness. Some such lateral movement can be seen in the finite element model in Figure 18.

### *6.4. Influence of Structural Silicone Sealant*

The magnitudes of moments about the longitudinal axes of the mullions are compared in Table 1. It can be seen that, compared to the moment due to wind load on the webs and flanges, the moment induced in the structural sealant is of secondary importance. For the sake of simplicity, the model proposed in Equations 21 to 23 ignores the moment and also the shear force in the sealant. Since the sealant resists lateral movement and resists rotation, it is to be expected that, for cases in which the lateral deflection of the mullion's interior flange is large, the analytical prediction will be an overestimate. For use in design, the model is therefore conservative.

### 6.5. Analytical and Numerical Predictions Compared

In Table 2, the algebraic predictions are compared with the results of the finite element study. It is to be expected that, because Equations 21 to 23 do not consider the torsional or shear resistance of the structural sealant, as the magnitude of the mullion’s rotation and lateral deflection increases, so the analytical forecasts will be overestimates. This expectation is consistent with the results in Table 2. Only one curtain wall design has been modelled, and therefore claims regarding the analytical method’s general applicability must be made with some caution. That said, it appears that lateral movements of a split mullion’s interior flanges can, for practical purposes, be estimated conservatively using Equations 21 to 23.

Table 2: Comparison of results obtained from the analytical and numerical models.

Phenomenon	Lateral Disp. of Int. Flange (mm)		References
	Male	Female	
Finite element prediction.	8.29	4.04	Section 4. Figure 18.
Sum of rotation and bending effects due to pressure equalisation.	12.99	3.60	Equation 21.
Sum of rotation and bending due to pressure equalisation, and also rotation due to moment transmitted through structural silicone sealant.	11.1	3.47	Moment from Equation 3, less moment from Equation 12. Lateral movements: due to rotation from Equations 4, 5 and 6; due to bending from Equation 7

### 6.6. Structural Silicone Sealant as a Torsional Brace

A question of interest to curtain wall designers [38] is whether or not a structural silicone sealant connection to glass is, on its own, effective as a torsional brace for a mullion extrusion. For the particular curtain wall system considered in this investigation, the answer is that the glass and sealant provide adequate torsional bracing to prevent lateral torsional buckling. The minimum torsional stiffnesses needed to prevent LTB, from Equation 1, are 48 and 113 N.m per m length of profile, per radian, for the male and female extrusions

respectively. The stiffness of the sealant connection, from Equation 12, is 174 N.mm/(mm.radian). While this is not necessarily the case for every curtain wall mullion shape and for every structural silicone bite, there is nothing in these comments to suggest that a structural silicone sealant joint will be ineffective as a lateral, rather than torsional, brace.

## 7. Conclusions

The majority of today's curtain walls are unitised systems made up of pre-fabricated panels [9, p. 82], whose principal framing members, the mullions, are slender aluminium extrusions. The cavities within these profiles ventilate to the outside of the building, and therefore wind pressure acts upon their webs. Curiously, these loads are not mentioned in the published literature.

In this investigation, the various different physical processes that cause a mullion's interior flanges to move laterally, or parallel to the wall, have been examined analytically. A new algebraic model has been proposed, in Equations 21 to 23, to describe the most significant of these effects, which are rotation about a longitudinal axis and flexure about the cross section's weak axis. Using these new expressions, a facade designer can calculate whether lateral movement of flanges will affect the serviceability of a male and female extrusion pair. In particular, the analysis can be used to reveal whether disengagement will occur at a mullion's central air seal.

An existing curtain wall system has been studied, and it has been shown that the applied moments, which twist the mullions about their prismatic axes, are large in comparison with any twisting moment needed to prevent lateral buckling of the compression flange. It is suggested that this finding will apply to unitised mullion designs in general. So, if Equations 21 to 23 show that, at full design load, a mullion extrusion's lateral movement is small, it follows that the profile is resistant to lateral torsional buckling. This new analysis may therefore obviate the need for the sort of LTB checks that are mandated by current design codes, which are time consuming and therefore expensive to perform.

Descriptions of the movement of a mullion's flange are complicated by the near-universal presence of structural sealant [37], which is used to bond the member's outer flange to the glass or other sheet material at the wall's exterior face. Because Equations 21 to 23 ignore the forces transmitted to the mullion by the sealant, it is to be expected that, for cases in which lateral movements are large, the predicted deflections will be greater than those that will occur in reality. The results obtained from a finite element model are consistent with this expectation. For design purposes, the proposed algebraic model is therefore conservative.

Previous research has shown that, even when custom curtain walls are developed specifically for a particular building, they often contain more aluminium than is structurally necessary [15]. It is hoped that, with a new model of the forces acting upon the mullions, together with this paper's new and reasonably simple expressions for structural analysis, it will be easier for facade engineers to design extrusions in which metal is used efficiently. Minimising material usage is always desirable, as it is a way to control building cost. For aluminium, whose embodied energy is much greater than that of other common building materials [16, p. 10], there is also a strong environmental incentive to use the metal sparingly. It is already known that, if the techniques proposed in this paper will help the curtain wall industry to reduce the mass of metal in its products, then the monetary savings, and also the reduction in greenhouse gas emissions, will be substantial [17, p. 24].

## **8. Acknowledgements**

The authors are grateful for the technical data and generous practical assistance provided by Mr. James Chant, Chairman of Seapac Philippines, and also for the valuable comments given by Engineer Leo Goco of Mott MacDonald's facade engineering group, who reviewed an early draft of this paper. The help given during the finite element study by Engineer Wellie Valdez, of PTCC Facade Design, is acknowledged with thanks.

## References

- [1] Ziemaiian RD, editor. Guide to Stability Design Criteria for Metal Structures. 6 ed.; John Wiley & Sons; 2010. ISBN 978-0-470-08525-7.
- [2] Yura JA, Helwig TA. Bracing for Stability; 1995. Document number RR3305.
- [3] Aluminum Association. Aluminum Design Manual; 2010.
- [4] Wigginton M. Glass in Architecture. Phaidon; 1996. ISBN 0 7148 2922 6.
- [5] Wurm J. Glass Structures: Design and Construction of Self-Supporting Skins. Birkhäuser Verlag AG; 2007. ISBN 978-3-7643-7608-6.
- [6] AJJ Glass Ltd.. Flat Tempered Glass. 2017. URL: <http://www.ajjglass.com/tempered-glass.html>; accessed 1 August 2017.
- [7] Saint-Gobain. Glass to the Max: 18m. Germany; 2016. URL: <https://www.saint-gobain-facade-glass.com/sites/default/files/Resources/BrocureOverlengthSGTG-Copy.pdf>.
- [8] Pulling LL, Muessel DC, Wille HS. Wall construction. 1962. URL: <http://www.google.com/patents/US3037591>; US Patent 3,037,591.
- [9] Yuanda China Holdings Limited. Global Offering; 2011. URL: [www.hkexnews.hk/listedco/listconews/sehk/2011/0420/02789\\_1057382/EWF114.pdf](http://www.hkexnews.hk/listedco/listconews/sehk/2011/0420/02789_1057382/EWF114.pdf); (Document available from Hong Kong Stock Exchange).
- [10] Center For Window and Cladding Technology. Technical Update No. 7: Buckling of Curtain Wall Mullions; 2002.
- [11] Aluminum Association. Aluminum Design Manual; 2015.
- [12] Skejić D, Lukić M, Buljan N, Vido H. Lateral torsional buckling of split aluminium mullion. Key Engineering Materials 2016;710:445–50. doi:10.4028/www.scientific.net/KEM.710.445.

- [13] Clift CD, Austin WJ. Lateral buckling in curtain wall systems. *Journal of Structural Engineering* 1989;115(10):2481–95. doi:10.1061/(ASCE)0733-9445(1989)115:10(2481).
- [14] Goco LT. Rationalizing assumptions for evaluating the lateral torsional buckling strength of aluminium mullion extrusions by EN1999 and AA ADM. Master’s thesis; Bath University, UK; 2017. URL: <https://www.bath.ac.uk/library/dissertations/index.php?programme=MSc+Architectural+Engineering%3A+Faade+Engineering>.
- [15] Lee AD, Shepherd P, Evernden MC, Metcalfe D. Optimizing the Cross-Sectional Shapes of Extruded Aluminium Structural Members for Unitized Curtain Wall Facades. *Structures* 2017;10:147–56. doi:10.1016/j.istruc.2017.03.002.
- [16] Hammond G, Jones C. Embodied Carbon: The Inventory of Carbon and Energy (ICE). Bath University and BSRIA; 2011. ISBN 978 0 86022 703 8.
- [17] Lee AD, Shepherd P, Evernden MC, Metcalfe D. Optimizing the architectural layouts and technical specifications of curtain walls to minimize use of aluminium. *Structures* 2017;13:8–25. doi:10.1016/j.istruc.2017.10.004.
- [18] Wang Y. Structural Behavior and Design of Two Custom Aluminum Extruded Shapes in Custom Unitized Curtain Wall Systems. Master’s thesis; University of Cincinnati, USA; 2006. URL: [https://etd.ohiolink.edu/!etd.send\\_file?accession=ucin1147722350](https://etd.ohiolink.edu/!etd.send_file?accession=ucin1147722350).
- [19] Euler L. *Methodus Inveniendi Lineas Curvas Maximi Minimive Proprietate Gaudentes*. Bousquet; 1744. For English translation see Ref. [20].
- [20] Oldfather WA, Ellis CA, Brown DM. Leonhard Euler’s Elastic Curves. *Isis* 1933;20(1):72–160. doi:10.1086/346767; English translation of Ref. [19].

- [21] Timoshenko S. History of Strength of Materials. McGraw-Hill; 1953. ISBN 0-486-61187-6.
- [22] Center For Window and Cladding Technology. Technical Note No. 6: The Principle of Pressure-Equalization; 2000.
- [23] American Architectural Manufacturers Association. The Rain Screen Principle and Pressure-Equalized Wall Design. 2012.
- [24] Raymond J. Roark and Warren C. Young and Richard G. Budynas. Roark's Formulas for Stress and Strain. 7 ed.; McGraw-Hill; 2002. ISBN 0-07-072542-X.
- [25] Xiang C, Luo ACJ, Seaburg P, Crain R. On the computation of the cross-section properties of arbitrary thin-walled structures. Proceedings of the 16th International Specialty Conference on Cold-Formed Steel Structures 2002;1:602–15. URL: <http://scholarsmine.mst.edu/isccss/16iccfss/16iccfss-session9/1>.
- [26] Fong J, Vanni W. Warping Constant of Open Section with Arbitrary Profile Geometry; 2010. URL: [http://www.cranereparengineer.com/Torsional%20Warping%20Constant%20\(Cw\)/OpenWarpingConst.pdf](http://www.cranereparengineer.com/Torsional%20Warping%20Constant%20(Cw)/OpenWarpingConst.pdf).
- [27] van Leeuwen R. Cross-Section Analysis in Python; 2017. URL: <https://robbievanleeuwen.github.io/assets/cross-section.pdf>.
- [28] Levy S. Bending of Rectangular Plates with Large Deflections; 1942. URL: <https://ntrs.nasa.gov/search.jsp?R=19930081641>; NACA Technical Note 846.
- [29] Föppl A. Vorlesungen Über Technische Mechanik. Druck und Verlag von B.G. Teubner; 1907. URL: <https://archive.org/details/vorlesungenbert25fpgoog>.
- [30] von Kármán T. Festigkeitsprobleme im maschinenbau. In: Klein F, Müller C, editors. Encyklopädie der Mathematischen Wissenschaften. Druck und



Verlag von B.G. Teubner; 1910, p. 311–85. URL: <https://archive.org/details/p4encyklopdieder04akaduoft>; 1907-1914 Edition.

- [31] Ciarlet PG. A justification of the von kármán equations. *Archive for Rational Mechanics and Analysis* 1980;73:349–89. doi:10.1007/BF00247674.
- [32] Beason WL. A Failure Prediction Model for Window Glass. PhD Thesis; Texas Tech University; 1980. URL: <https://ttu-ir.tdl.org/ttu-ir/handle/2346/10495>.
- [33] Navier CLMH. Extrait des Recherches sur la Flexion des Plans Élastiques. *Bulletin des Sciences par la Société Philomatique de Paris* 1823;–:92–102.
- [34] Navier CLMH. Sur les Lois de l'Équilibre et du Mouvement des Corps Solides Élastiques. *Bulletin des Sciences par la Société Philomatique de Paris* 1823;–:177–81.
- [35] Beason WL, Morgan JR. Glass failure prediction model. *Journal of Structural Engineering* 1984;110(2):197–212. doi:10.1061/(ASCE)0733-9445(1983)109:2(489).
- [36] AS 1288. Glass in Buildings – Selection and Installation; 2006. URL: <http://www.standards.org.au>.
- [37] ASTM C1401. Standard Guide for Structural Silicone Sealant Glazing; 2014. doi:10.1520/C1401-14.
- [38] Lee AD, Shepherd P, Evernden MC, Metcalfe D. Measuring the effective young's modulus of structural silicone sealant in moment-resisting glazing joints. *Construction and Building Materials* 2018;181:510–256. doi:10.1016/j.conbuildmat.2018.06.038.
- [39] Dow Corning Corporation. Product Information: Dow Corning 983 Structural Glazing Sealant; 2012. URL: <http://www.dowcorning.com/content/publishedlit/63-1110.pdf>; Dow Corning Form Number: 63-1110C-01.

- [40] Gavin HP, Pye J. User Manual and Reference for Frame3DD: A Structural Frame Analysis Program; 2013. URL: <http://www.sourceforge.net/projects/frame3dd>.
- [41] EDF R&D. Code\_Aster: Analysis of Structures and Thermomechanics for Studies and Research; 2010. URL: [http://www.code-aster.org/UPLOAD/DOC/Presentation/plaquette\\_aster\\_en.pdf](http://www.code-aster.org/UPLOAD/DOC/Presentation/plaquette_aster_en.pdf).
- [42] Open Cascade SAS (Euriware Group). Salome: the open source integration platform for numerical simulation. 2018. URL: <http://www.salome-platform.org>.
- [43] ASTM E1300. Standard Practice for Determining Load Resistance of Glass in Buildings; 2004. doi:10.1520/E1300-04.